

Title: **HERSCHEL Straylight Calculation Results**

CI-No: 100 000

Prepared by: A. Frey / H. Hartmann Date: 24.10.2003

Checked by: E. Hoelzle

Product Assurance: R. Stritter

Configuration Control: A. von Ivady

Project Management: W. Rühle

Copying of this document, and giving it to others and the use or communication of the contents thereof, are forbidden without express authority. Offenders are liable to the payment of damages. All rights are reserved in the event of the grant of a patent or the registration of a utility model or design.

Issue	Date	Sheet	Description of Change	Release
1	10.06.02	1-37	First issue	
2	18.10.02	1-74	Completely revised issue	
3	24.10.03	1-86	Completely revised issue	

Table of contents

1	INTRODUCTION	5
2	REFERENCE DOCUMENTS	5
3	STRAYLIGHT REQUIREMENTS	6
4	MODEL DESCRIPTION	7
	4.1 GENERAL OVERVIEW	7
	4.2 ASAP INSTRUMENT MODELS	10
	4.3 TELESCOPE MODEL	18
	4.4 M1 BAFFLE	24
	4.5 DIMENSIONS USED	26
	4.6 EMISSIVITIES AND TEMPERATURES USED	27
5	SUPPLEMENTARY CALCULATIONS	28
	5.1 OBSCURATION CALCULATIONS	28
	5.2 STRAYLIGHT FROM LOU WINDOWS VIA MULTIPLE REFLECTIONS WITHIN THE THERMAL SHIELDS	30
	5.3 CALCULATION OF AN EFFECTIVE EMISSIVITY FOR THE GAP BETWEEN SUNSHADE AND M1	35
6	THERMAL EMISSION (SELF EMISSION)	43
	6.1 INTRODUCTION	43
	6.2 DIFFRACTION CALCULATIONS	44
	6.2.1 Introduction	44
	6.2.2 Diffraction at the rim of apertures in the telescope focal surface	47
	6.2.3 Diffraction at the rim of the secondary mirror with the gap near the sunshade as thermal source	48
	6.3 THERMAL EMISSION FROM THE HIFI OSCILLATOR WINDOW	55
	6.4 RESULTS	57
7	SOURCES OUTSIDE THE FOV (SUN, EARTH, MOON)	65
	7.1 SPECULAR PATHS FROM MOON AND EARTH	65

7.2	SCATTER PATHS FROM MOON AND EARTH	72
7.3	SOLAR IRRADIATION	72
8	SOURCES INSIDE THE FOV	73
9	SUMMARY OF CHANGES NOT FULLY REFLECTED BY PRESENT CALCULATIONS	74
10	SUMMARY ON STRAYLIGHT	75
11	APPENDIX: SCATTERING MODELS USED FOR THE CALCULATIONS	76

1 Introduction

This TN presents the results of the Straylight Analysis for HERSCHEL.

2 Reference Documents

RD1	Herschel Telescope Straylight Analysis	HER.NT.017.T.ASTR, issue 3, 01 Okt 02
RD2	Earth & Moon Radiometric Hypotheses for Straylight	H-P-1-ASPI-TN-0216, issue 2, 30 04 02
RD3	Herschel Straylight Analysis	H-P-2-ASPI-TN-0379, issue 1, 27 Sep 02

3 Straylight Requirements

The requirements as can be found in the IID-A, issue 3/0, are described below:

For the spacecraft design w.r.t. straylight for the Herschel instruments an integrated approach has been selected. This means that the instrument optical layout is included in the system straylight analysis. This approach allows to directly provide the straylight level originated from the various sources at the detector level.

The system straylight requirements are given therefore directly as the straylight reaching the detector level. The system will provide the following maximum straylight over the full operational wavelength:

Scattered light (source outside the telescope FoV)

Taking into account the worst combination of the Moon and the Earth positions w.r.t. LOS of the telescope with maximal:

- Sun - S/C - Earth angle of 37°
- Sun - S/C - Moon angle of 47°
- Sun - S/C - LOS angle of 60° to 120° (in x-z plane)
- Sun - S/C - LOS angle of $\pm 1^\circ$ (about x = roll)

the straylight shall be: < 1.0% of background radiation induced by self-emission of the telescope.

Sources inside FOV:

Over the entire FOV at angular distances $3'$ from the peak of the point-spread-function (PSF), the straylight will be: < 1×10^{-4} of PSF peak irradiance (in addition to level given by diffraction).

Self-emission

The straylight level, received at the defined detector element location of the PLM/Focal Plane Unit Straylight model by self emission (with "cold" stops in front of PACS and SPIRE instrument detectors), not including the self emission of the telescope reflectors alone, will be 10% (tbc) of the background induced by self-emission of the telescope reflectors.

4 Model Description

4.1 General Overview

The present status of the overall ASAP model is displayed in figure 4.1-1. A detailed plot of the design from the M1-baffle down to the instrument shield is shown in figure 4.1-2.

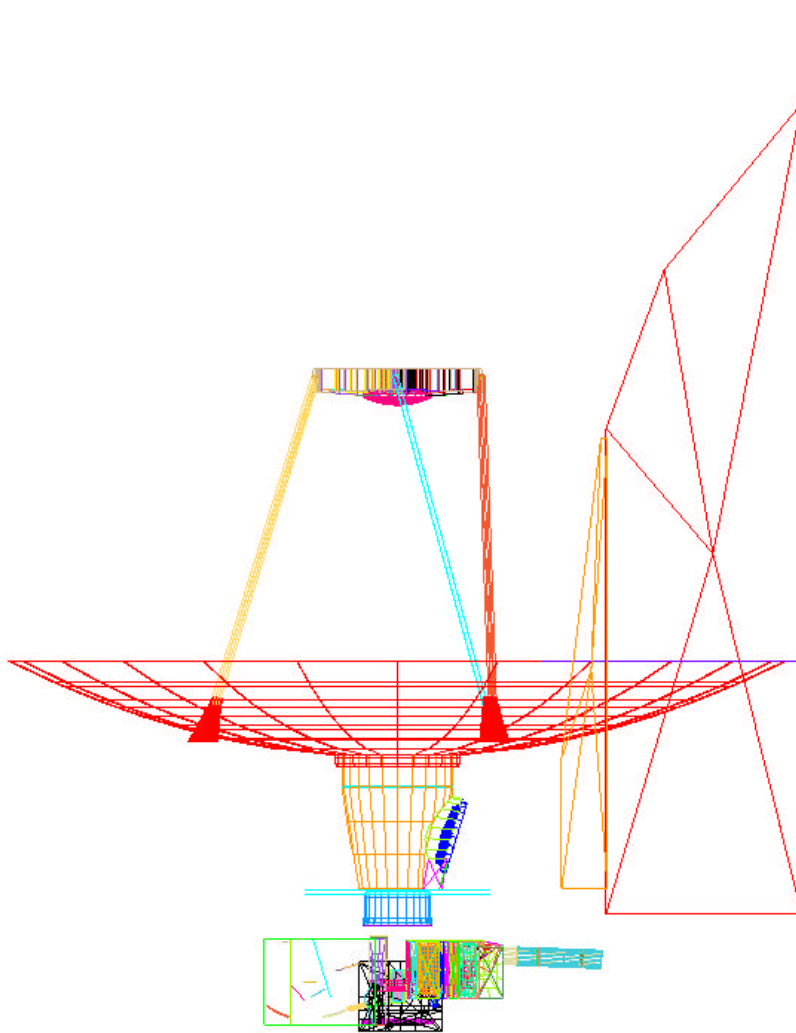


Figure 4.1-1: Overall configuration plotted with the present ASAP model

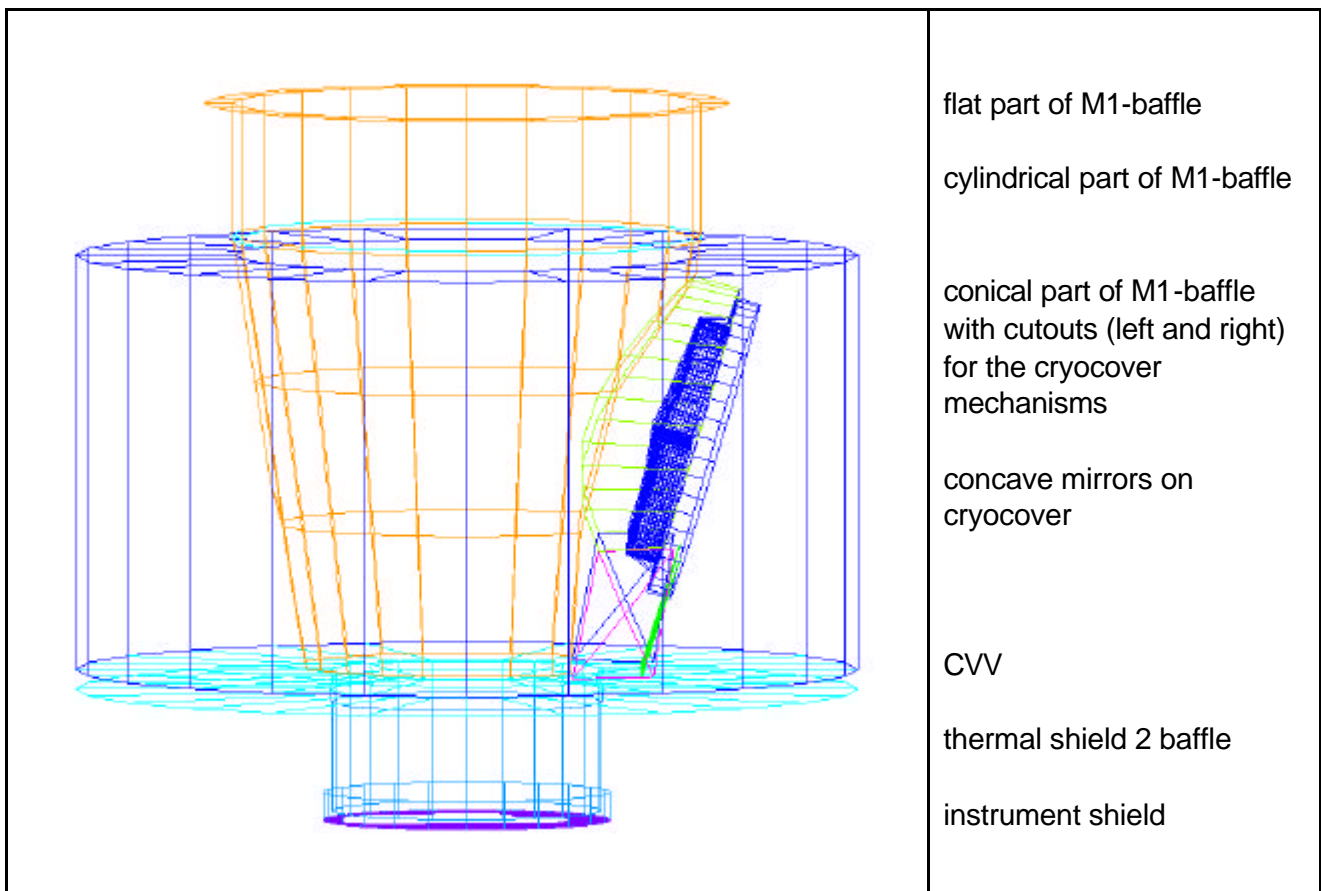


Figure 4.1-2: Detail of design from M1-baffle down to the instrument shield

Four ASAP models have been received, all of them were integrated into the total optical ASAP model of Herschel

- the telescope model
- the SPIRE model
- the PACS model
- the HIFI-model

The rest of Herschel to be modeled for the straylight analysis comprises

- the sunshade
- the cryostat part near the cryocover
- the baffle between cryostat and telescope (M1-baffle)
- the thermal and instrument shields (the parts above the instruments).

this page left intentionally blank

4.2 ASAP instrument models

The instrument ASAP models are displayed in the next figures:

- the SPIRE model in figure 4.2-1
- the PACS model in figure 4.2-2
- the HIFI-model in figure 4.2-3.

Several iterations have been performed for SPIRE and PACS in order to have sufficient model fidelity.

Compared to issue 2 of this technical note, there was a considerable change in the ASAP model for PACS

- there is a new data basis for the modeling of all mirrors, i.e. an Excel sheet with mirror data; the ASAP commands for the mirrors have been set up by Astrium; the difference to the earlier mirror geometry mainly affects the mirror limitations (not the curvatures)
- all calibration mirrors are modeled now
- the entrance opening is modeled now.

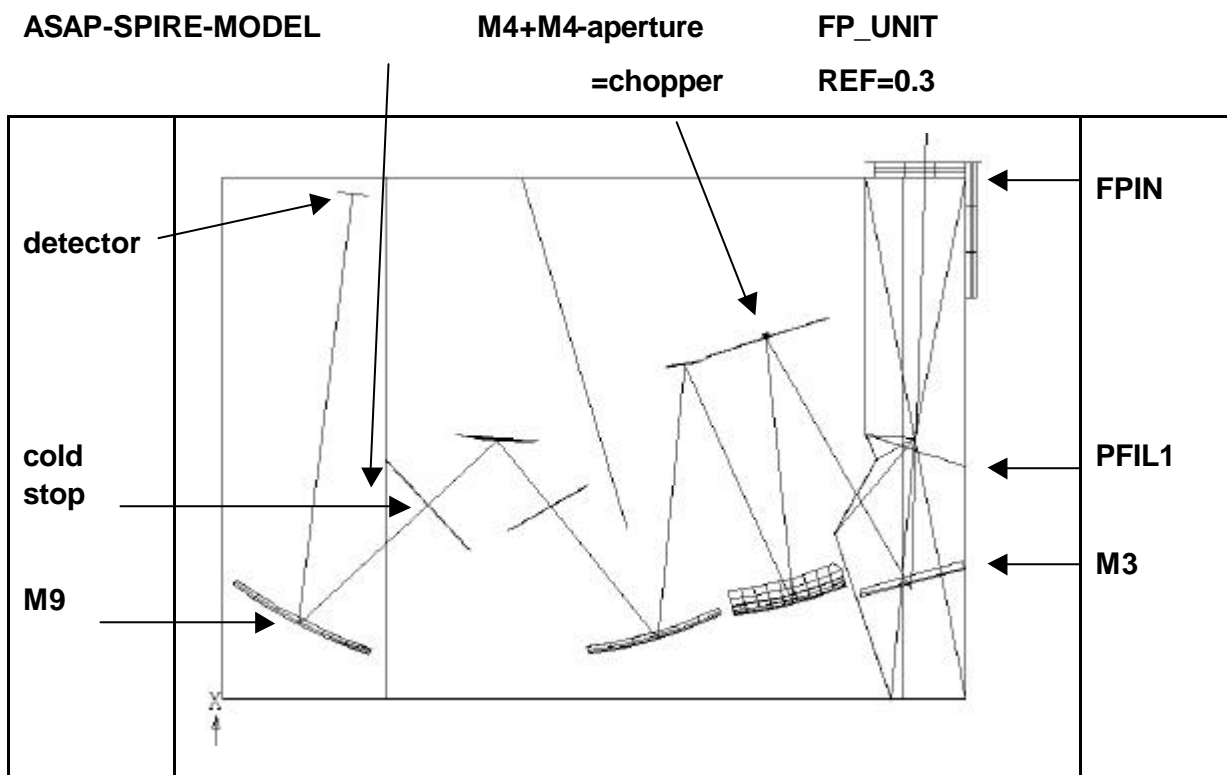


Figure 4.2-1: ASAP SPIRE model; it represents a singular path towards one of the detectors of the photometer. This photometer path is representative for the straylight sensitive paths within SPIRE.

ASAP PACS-MODEL → cold stop chopper

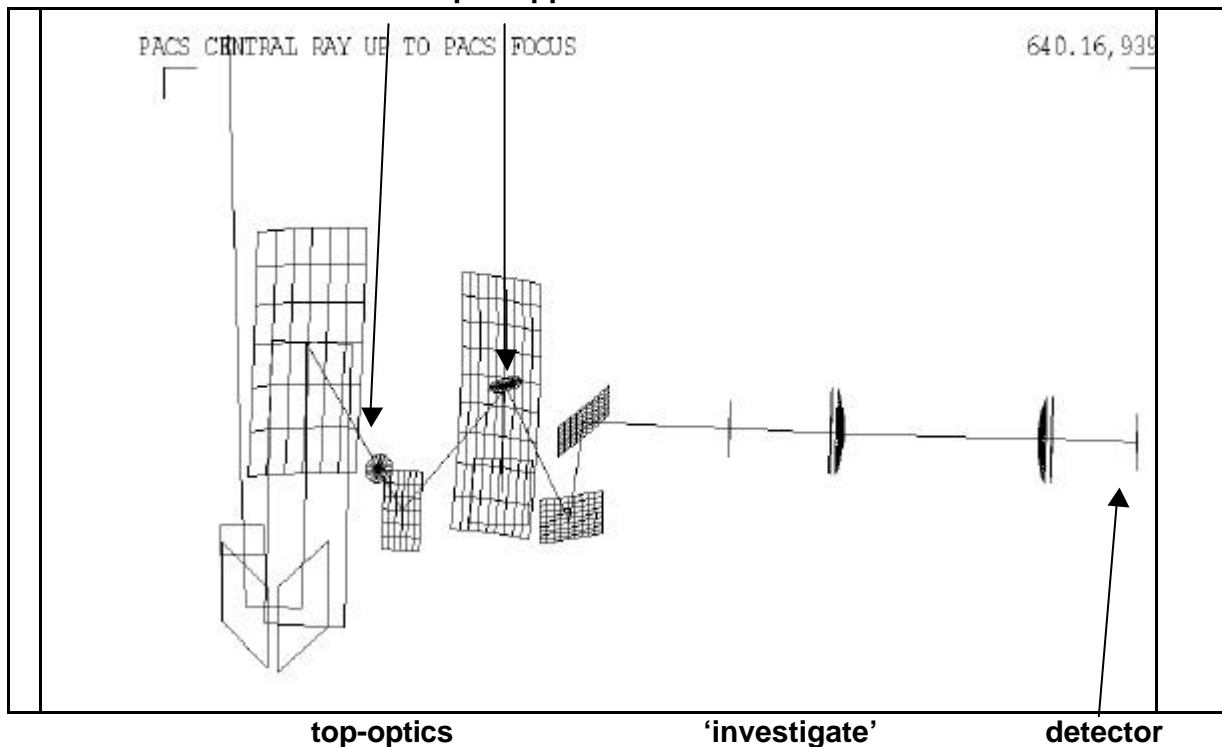


Figure 4.2-2: ASAP PACS model. Only the optics is shown, without structural elements. A specific detector path has been selected as representative for straylight.

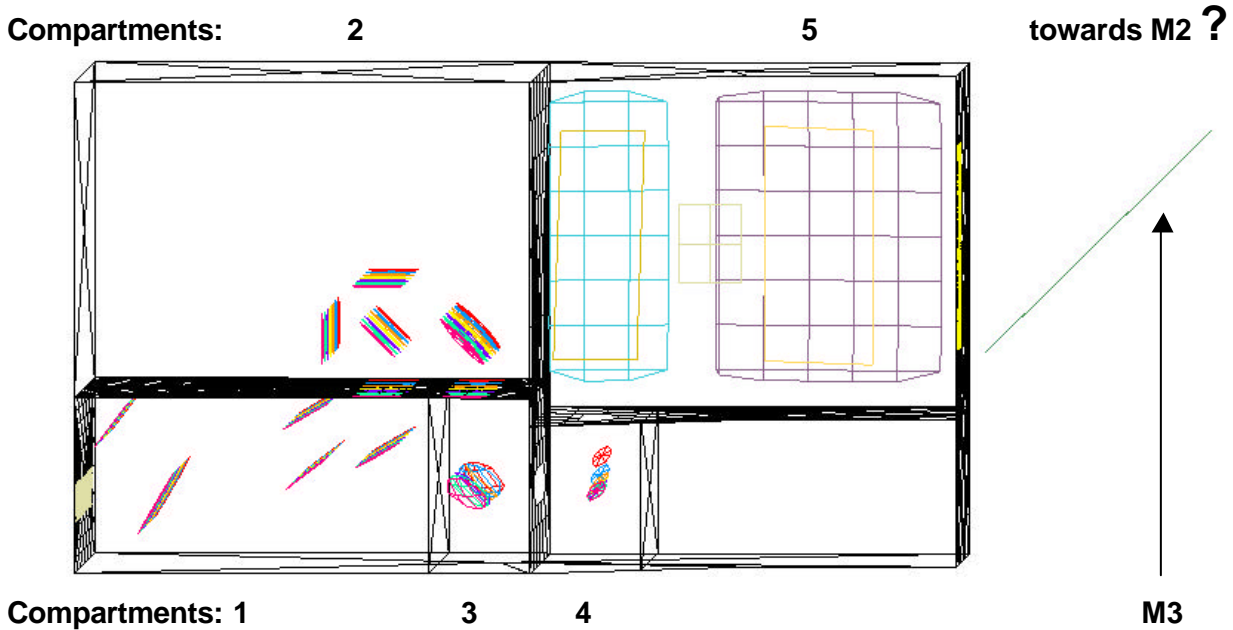


Figure 4.2-3 ASAP-HIFI model. HIFI is not straylight sensitive; it is included because it may influence straylight towards PACS and SPIRE. The compartment numbering is introduced in order to enable easier description of the straylight calculations. The compartment numbers increase from the local oscillator windows to the inner opening towards M3 and M2 (telescope secondary mirror).

There is an object-image relation between the hole within SPIRE M4 and the center of M2. This leads to a partial obscuration of some straylight contributions, as the calculations will show.

The optics design of SPIRE confines the acceptance cone for purely specular radiation very closely to the secondary mirror as a backward raytrace shows, only a very small fraction of the hexapod can be seen by the SPIRE detector (see figure 4.2-4).

The confinement of the acceptance cone for purely specular radiation is similar for PACS (not as close as for SPIRE); a backward trace from the PACS detector is shown in figure 4.2-5.

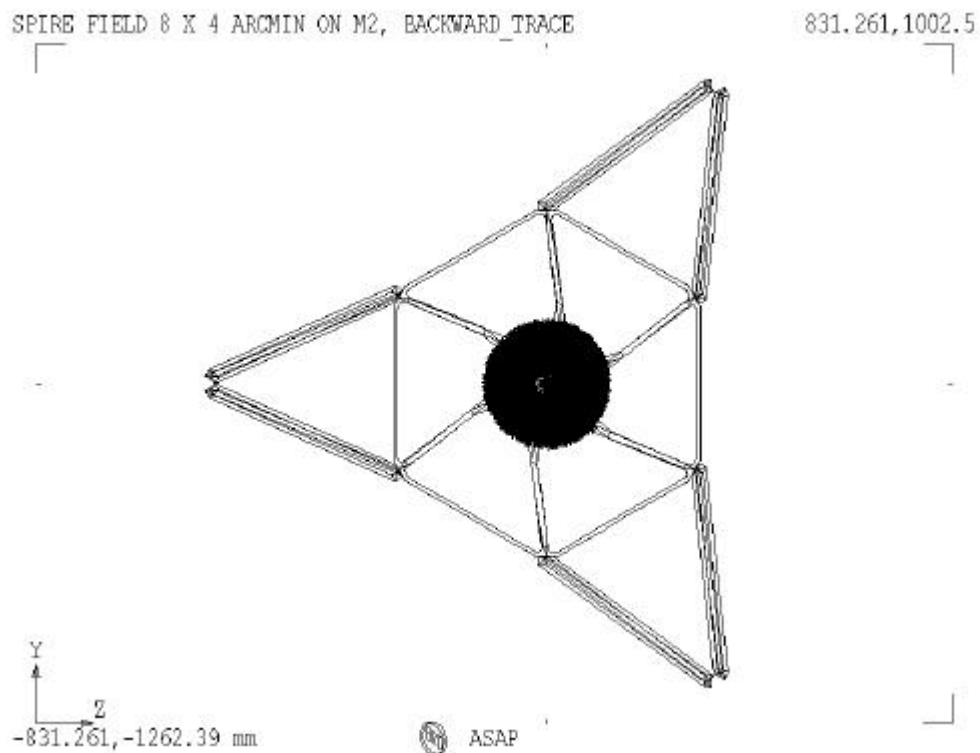


Figure 4.2-4: Backward trace onto M2 starting from the SPIRE detector

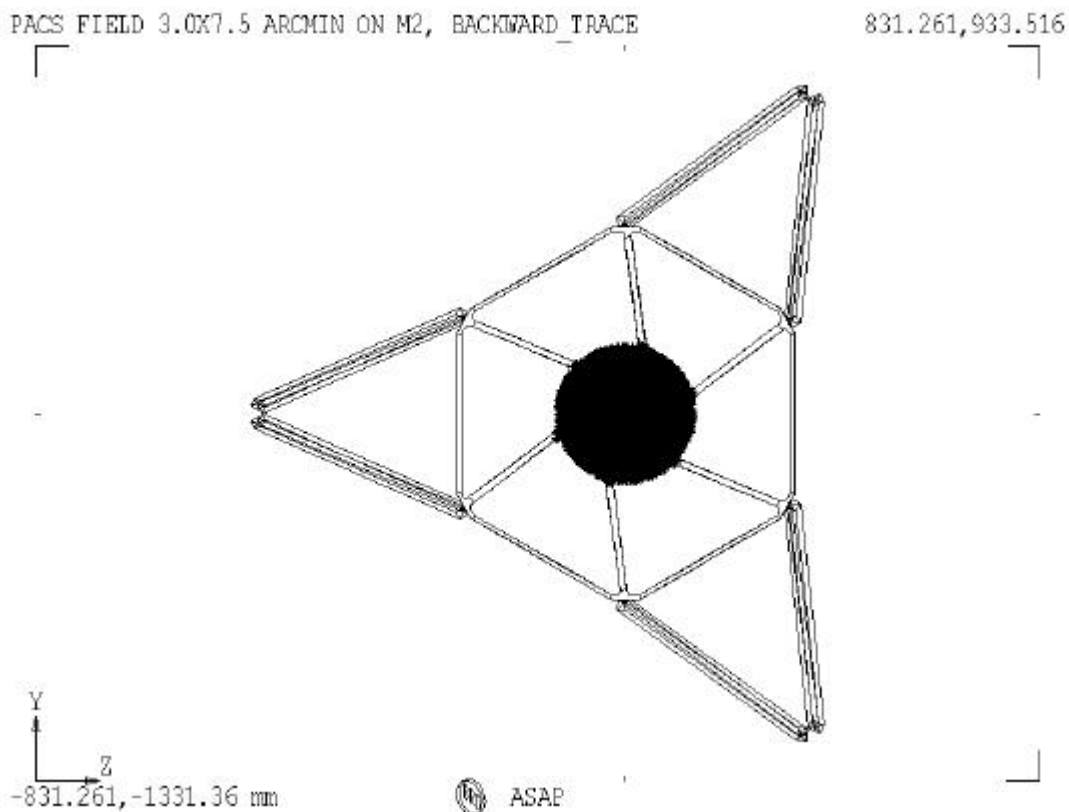
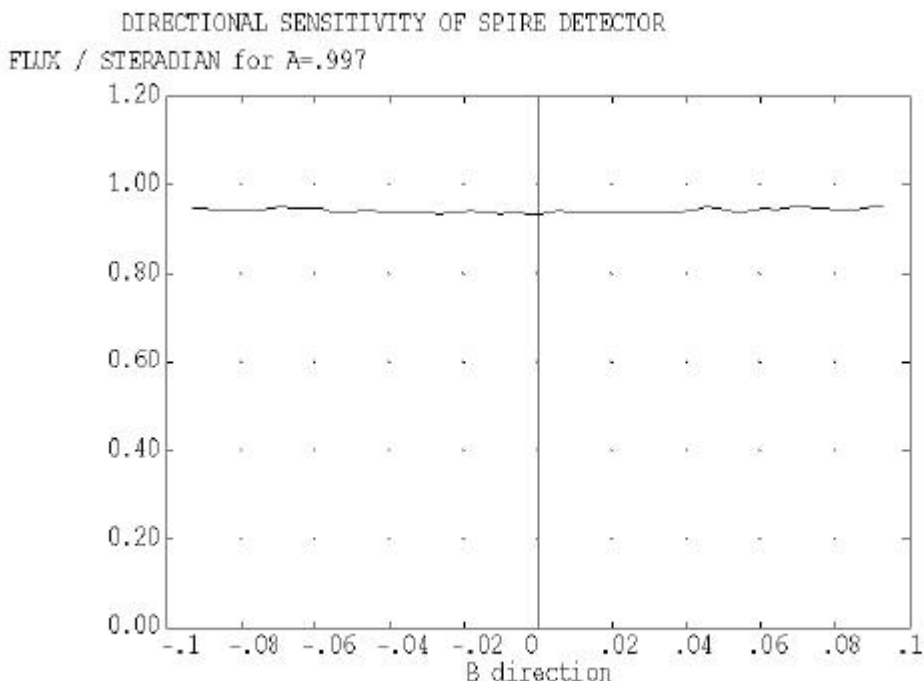


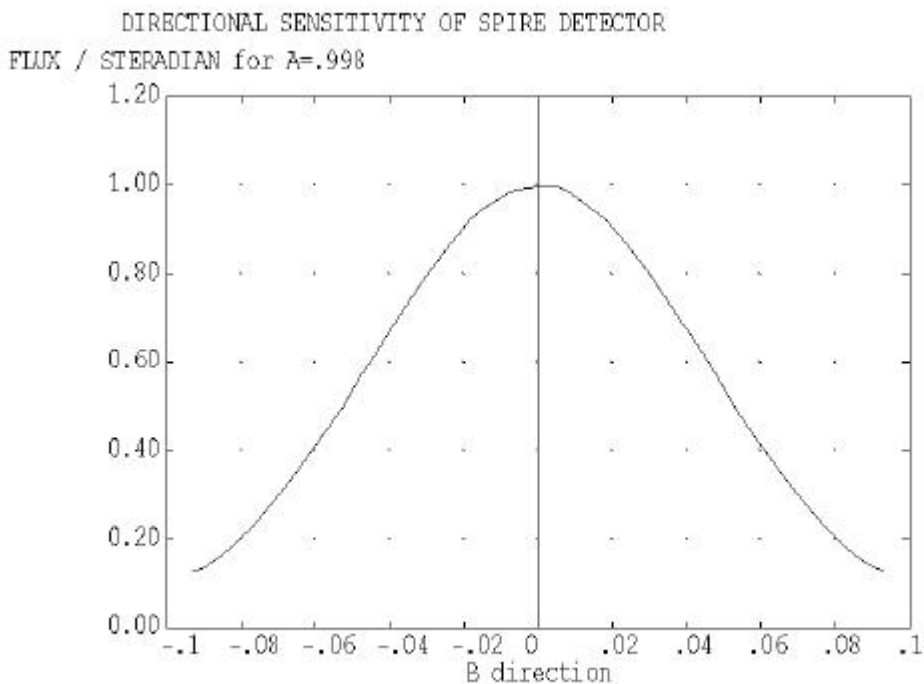
Figure 4.2-5: Backward trace onto M2 starting from the PACS detector

For the straylight calculations the instrument detectors labelled in figures 4.2-1 and 4.2-2 have been considered as representative for all detectors of the respective instrument:

The apodization effect (or edge taper) of the horns in front of the SPIRE detectors is included. For radiation impinging on the horns, this effect produces a change in sensitivity depending on the angle w.r.t. the horn axis such that the sensitivity decreases for increasing angles. Projected onto the pupils of SPIRE (cold stop, telescope secondary) there is a decrease of 8 dB, i.e. an edge taper of 8 dB. This edge taper is realized for the calculations with the apodization function of ASAP, this is a ray change in ASAP. Thus there is no change of objects in the ASAP SPIRE model. The effect of the ASAP apodization is displayed in figure 4.2-6. This is not just a graphical representation of a gaussian function, but the result of a raytrace with a beam starting at the telescope secondary and ending at the SPIRE detector. There the resulting radiant intensity (in direction cosine space) is displayed without and with apodization. All the new calculations in this issue 3 (i.e. those on thermal self emission) have been performed including the apodization for SPIRE.



ABSCISSA IS DIRECTION COSINE SPACE
 CURVE WITHOUT APODIZE FUNCTION FOR DIRECTIONAL SENSITIVITY



ABSCISSA IS DIRECTION COSINE SPACE
 CURVE WITH APODIZE FUNCTION FOR DIRECTIONAL SENSITIVITY

Figure 4.2-6: ASAP apodization function at SPIRE detectors (edge taper of 8 dB)

The scattering functions of the instruments are grouped into 2 categories:

- scattering function for mirrors
- scattering function for thermal filters.

Those for the mirrors were found within the delivered ASAP files. It will become clear later on that they do not play an important role, i.e. mirror scattering within the instruments does not dominate. Therefore the choice of parameters is not important.

The SPIRE mirror scattering function is displayed in figure 11.3-1 in the appendix. It is a particle model with many parameters determining the resulting scattering function. Two PACS mirror scattering functions have been delivered; as a worst case, the higher one has been selected (displayed in figure 11.2-1 in the appendix).

No scattering functions were delivered for thermal filters for PACS. In that case the scattering function was found not important, as a check we inserted an (arbitrarily selected) high function, i.e. a lambertian scatterer with $BSDF=0.1/\pi$ 1/sr at the place of the cold stop. No important scatter path resulted from this insertion.

For SPIRE a scattering function was received for the thermal filters 1 and 2 (see figure 11.3-5 in the appendix). This function had been measured as reflection function, the rays transverse it by transmission in Herschel. Here the thermal filter 1 may open important scattering paths as the chapters on thermal self emission will show. The reason for the imbalance between SPIRE and PACS with respect to the sensitivity on filter scattering is that the PACS thermal filter is more deeply buried within the instrument than thermal filter 1 of SPIRE.

The scattering functions received for the inner sides of the FP-unit (=input compartment) are displayed in figures 11.3-3 and 11.3-4 in the appendix.

4.3 Telescope model

The telescope models were established by Astrium France, they are described in detail in reference document RD1. Some characteristics and the evolution of changes are repeated here for sake of completeness.

The telescope model now contains the variants

- hexapod with rectangular legs
- hexapod with elliptical legs
- small scattercone with continuous slope change
- large scattercone with continuous slope change.

In issue 1 of the present TN the rectangular legs were included as baseline. Highly effective specular paths towards selected patches of the sky were detected for the rectangular legs.

Therefore the version with elliptical legs was introduced, it shall reduce these specular paths. The elliptical legs are modelled with a polygonal cross section with 24 sides. In issue 2 of the present TN all calculations (i.e. those on thermal self emission) have been performed with the version with elliptical legs.

The specular paths found for the elliptical version are more spreaded over the sky, however they represent less sensitive paths. A comment from the scientists states that the minor degree of spreading is favoured, so all the new calculations in this issue 3 (i.e. those on thermal self emission) had been performed with the version with rectangular legs.

The scattercone (also called antinarcissus) was introduced earlier as a reflector placed in the center of the M2 mirror with an extent such that it occupies the area which cannot be used by the Cassegrain telescope type for stellar radiation (central obscuration). The slope had been devised such that backreflections from instrument to M1-baffle via M2 do not occur. As consequence there was a discontinuous slope change from the M2-surface to the surface of the scattercone. While that discontinuity is favourable for avoiding views of the instruments towards the objects in the center of M1 (via M2), it is likely to produce problems for HIFI in terms of standing waves.

Numbers and figures for obscuration and straylight characteristics are listed in sections 5 and 6. Here the reflection behaviour of the three scattercone versions are displayed by the sequence of figures 4.3-1 through 4.3-3. There beams have been generated originating within SPIRE and PACS, these beam were traced backwards towards the M2-assembly. Similar figures have been presented in RD1 for the center of the FOV at the telescope system focus. The figures shown here use the following extreme beams from the edges (at $-Z$ and $+Z$) of the SPIRE and PACS fields.

color code in figures 4.3-1 through 4.3-3		
color	beam generated at	beam reflected by
blue	SPIRE, -Z side	scattercone, half at -Z
yellow	SPIRE, -Z side	M2, inner part near scattercone at -Z
black	PACS, +Z side	scattercone, half at +Z
red	PACS, +Z side	M2, inner part near scattercone at +Z

Many calculations in the earlier issue 2 have been performed with the versions with continuous scattercone (small and large).

The different versions have the following properties:

scattercone	small discontinuous	small continuous	large continuous
obscuration ratio, rectangular legs	≈7.7%	7.7%	10.3%
obscuration ratio, elliptical legs	≈8.7%	8.7%	11.3%
energy within 1 st dark ring of Airy disk	≈79%	79%	75%
standing waves (HIFI)	present	reduced	reduced
background homogeneity for chopping/nodding	better	worse	better
thermal self emission	lower	higher	lower

The evaluation by the scientists resulted in the favour of the small continuous scattercone, mainly because of the better (i.e. smaller) obscuration ratio and the reduced flux of standing waves. All calculations presented in this issue 3 involve the small continuous scattercone.

Another improvement is the abolishment of the chamfers at the transition between scattercone and M2-surface. These chamfers (having the shape of a roof with 45 degrees inclination) introduce a retroreflection in one plane. The programming code received from Astrium France had been changed such that the chamfers are removed (the original model contains them).

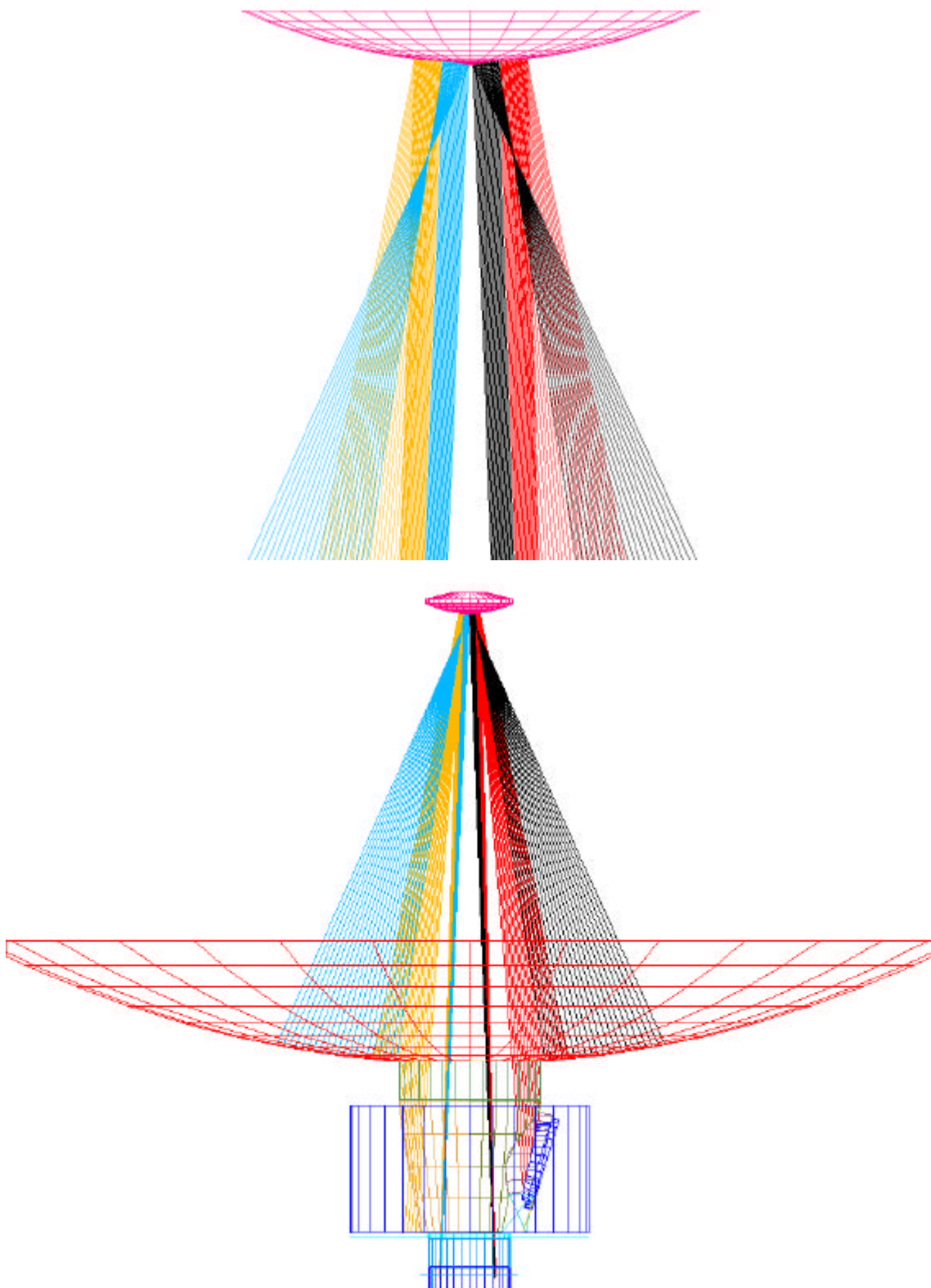


Figure 4.3-1: Back-reflections by the small discontinuous scattercone

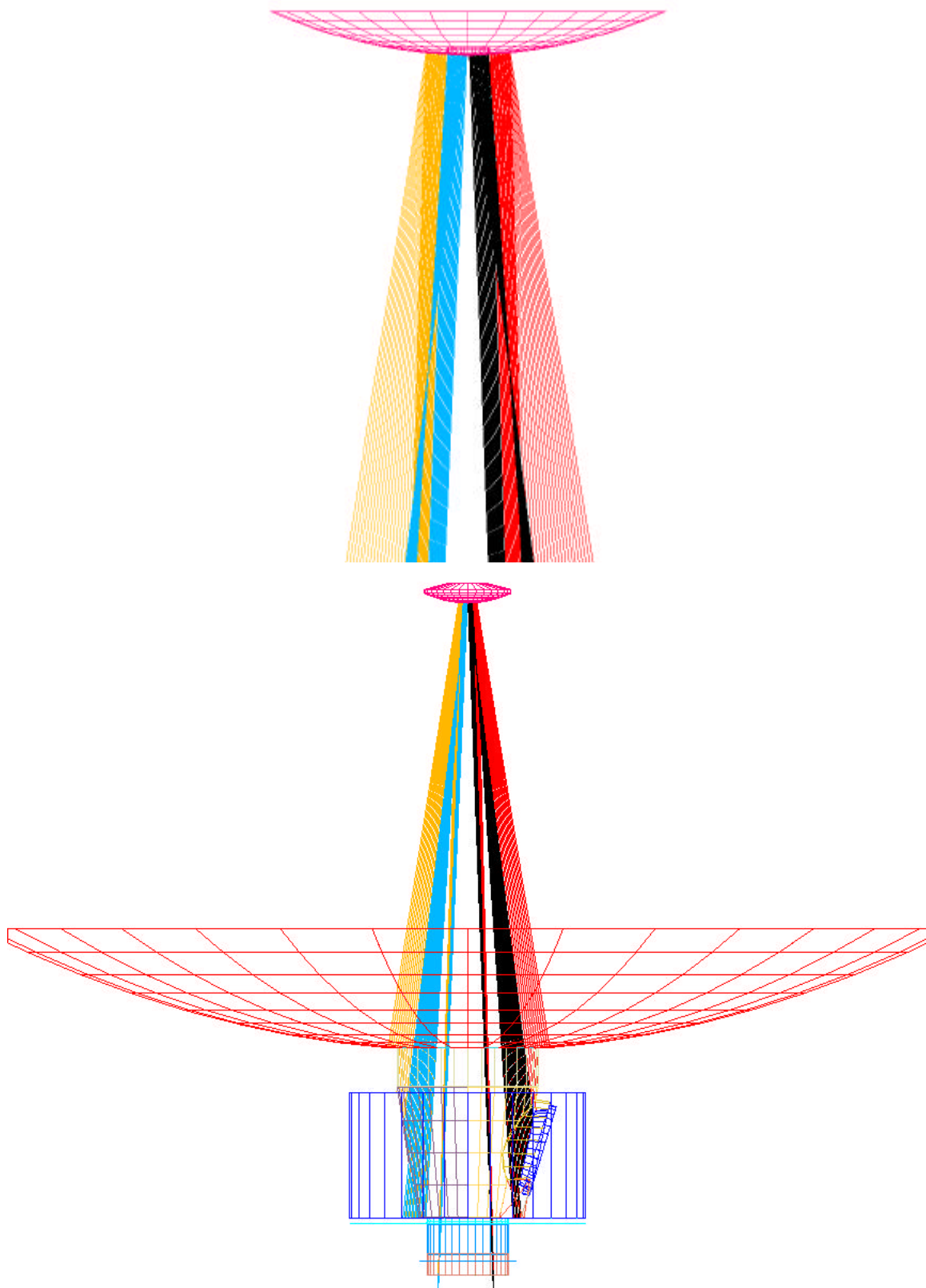


Figure 4.3-2: Back-reflections by the small continuous scattercone

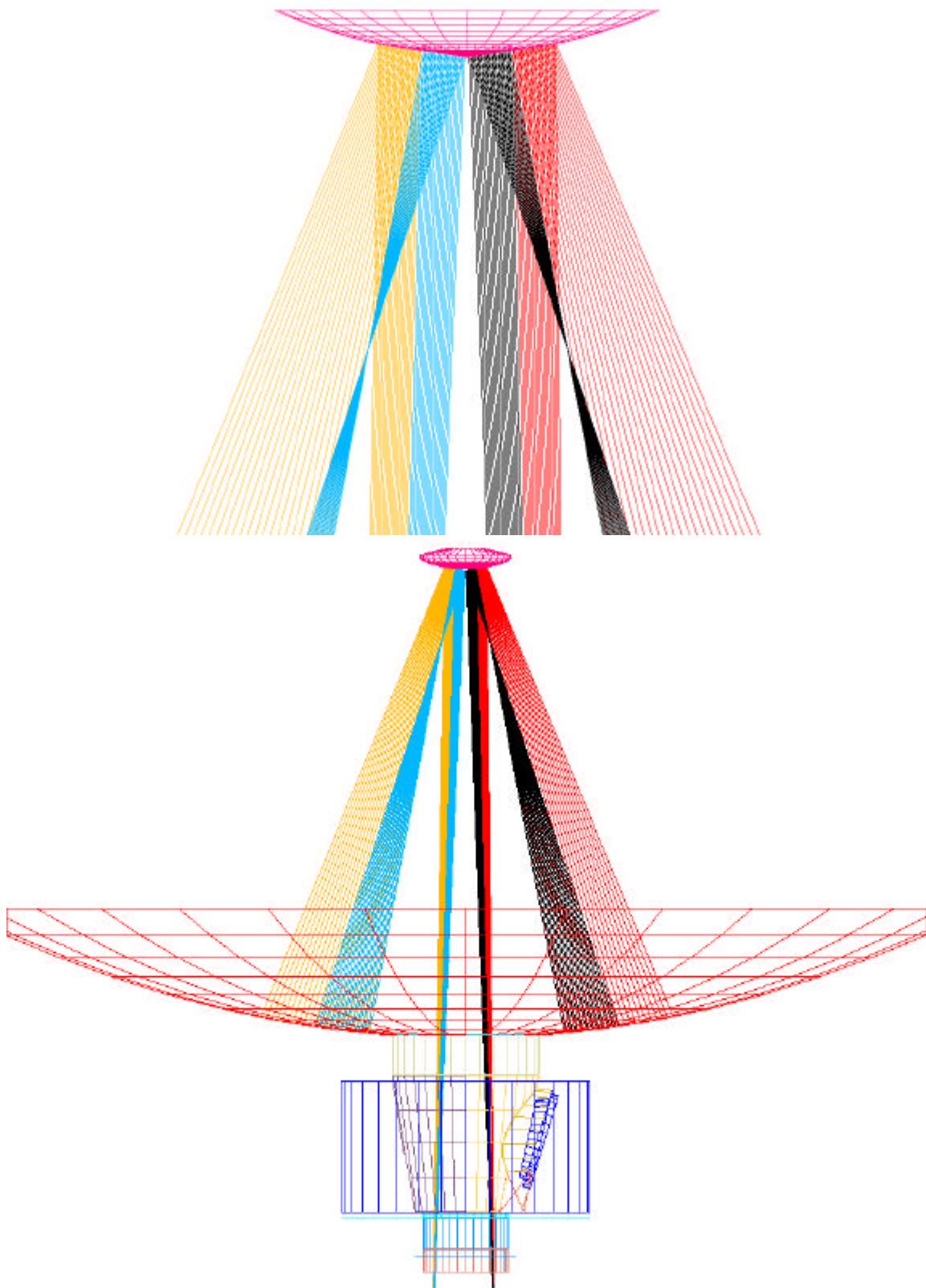


Figure 4.3-3: Back-reflections by the large continuous scattercone

The telescope barrel surfaces facing towards $-X$ -axis have been detected as effective reflecting surfaces for the HIFI instrument, the reflection produces undesirable standing waves. Therefore a change in the barrel surface limitation was introduced, see figure 4.3-4. The inclination of the surfaces is exaggerated there for sake of visibility. The corresponding change in the ASAP telescope model has been performed by ESTEC and is intergrated in the overall ASAP model. All calculations presented in this issue 3 include the inclinations shown in figure 4.3-4.

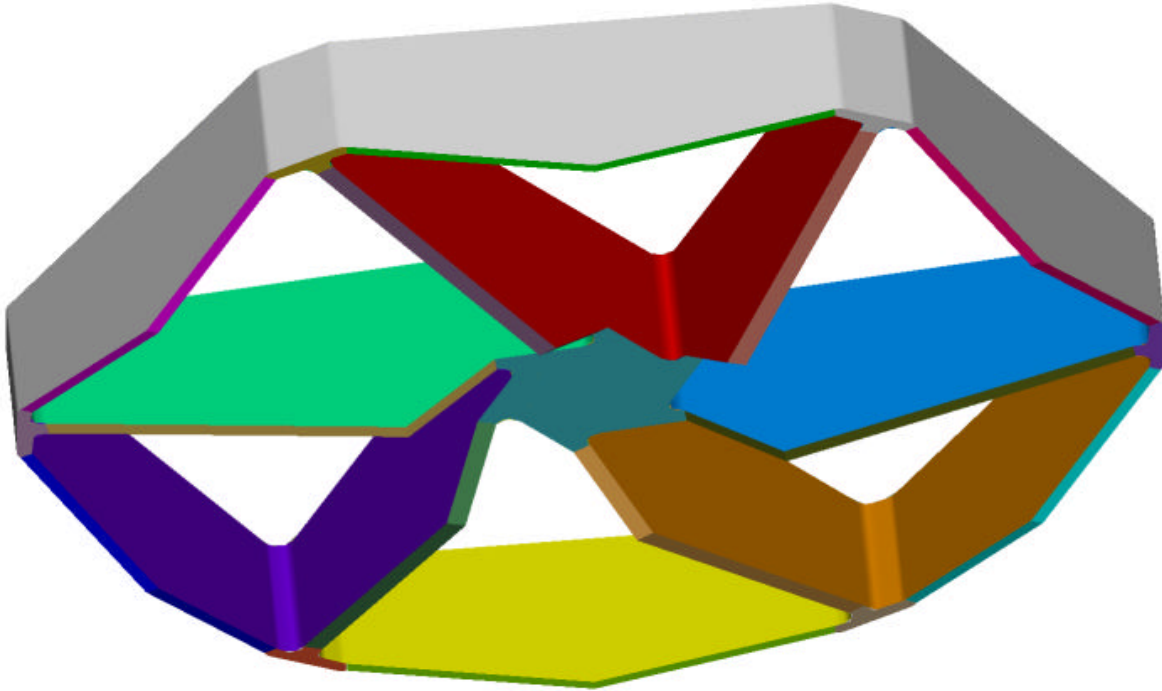


Figure 4.3-4: Change in inclination of the lower hexapod barrel surfaces (the inclination of the surfaces is exaggerated here for sake of visibility), this inclination shall reduce back reflections towards HIFI thereby reducing the standing waves.

A new telescope mirror scattering function (displayed in the appendix in figure 11.1-2) had been delivered by Astrium France shortly after completion of the calculations for issue 2. The new one is higher than the earlier one, it is the basis for all calculations for issue 3 (involving the telescope).

4.4 M1 Baffle

The space between the hole within the primary mirror and the cryostat requires attention, since an interface harmonization was necessary there (keyword M1-baffle). The design follows the rules:

- keep warm bodies far off the instrument beam
- avoid zigzag reflections with directions roughly parallel to the x-axis

Zigzag reflections near the y/z-plane are not as critical as they are not likely to reach the instruments. The mechanical needs result in some planes parallel to the Y/Z-plane (e.g. on top of the CVV), so some zigzag reflection paths cannot be avoided.

Also other components around the baffle set constraints, mainly the cryocover and the accessories necessary for its operation. The lower radius of the M1-baffle reflects the mechanical configuration there.

In issue 1 investigations have been performed for two different designs for the baffle within the centre of the telescope primary mirror (the M1-baffle),

- a cone-baffle
- a cylinder-baffle.

The progress in interface definition w.r.t. the inner rim of the telescope primary led to a restriction of the available diameter of 500 mm for the M1-baffle. Therefore a cylindrical shape has to be chosen for the upper part of the M1-baffle, since a continuous cone from the M1-vertex down to the CVV is not reasonable with an upper diameter of only 500 mm. The lower part can be made conical, the conical shape limits the thermal radiation transport towards the instruments. The resulting cone/cylinder-baffle has been shown already in figure 4.2-1. All the new calculations in issue 2 and issue 3 (i.e. those on thermal self emission) have been performed with that version of the M1-baffle.

The flat ring above the cylindrical part of the M1-baffle (see figure 4.1-2) is part of all calculations in this issue 3. A very recent change is the wish of HIFI for a conical shape of the innermost flat part of the M1-baffle. Meanwhile the flat shape has been abandoned and it was decided to give an upwards angle of 3.5 degrees +/- 2 degrees for the upper flat part of the M1 central baffle. The consequences are estimated to be small for general straylight, since it has been verified that no additional purely specular paths are introduced by this change.

Several gap closures have been introduced around the (open) cryocover. Thus the so-called 'inner cavity objects' (which have been treated in issue 1 as highly emissive objects) now mostly are low emissive objects, only a small ring around the cryocover has to be treated as highly emitting.

In connection with issue 1 there had been some discussion on the placement of the cryocover relative to the other Herschel components. Status on object positions is

- sun/earth/moon and sunshade at +Z
- cryocover and main mechanics at +Z
- rest of cryocover mechanisms at -Z
- PACS at +Z
- SPIRE at -Z.

The chopping beam motion of the instruments is desired to occur with as much homogeneous background as possible. Therefore the chopping motions are parallel to the X/Y-plane with no appreciable beam motion towards Z. The cryocover position at +Z complies with that intention. The consequence is a possible misbalance of straylight onto PACS and SPIRE from the thermal emitters mentioned.

The surface of the cryocover shall be adequate for establishing a predictable background for the ground tests, i.e. with the closed position of the cryocover. The options and selection of the details of this surface are reported in HP-2-ASED-TN-0076, issue 2. Baseline is now the option with concave mirrors for SPIRE and PACS. The corresponding ASAP commands for these mirrors are applied for all calculations in the present TN.

Three objects are planned to be black due to thermal reasons

- the short cone of the cryocover
- the thermal shield 2 baffle
- the instrument baffle (cylinder only).

Partially this choice is disadvantageous for straylight, nevertheless the priority has been given to the thermal reasons. The blackening most probably will be an anodizing process, not a sophisticated black color application (as planned for the instruments). Thus, at scientific wavelengths, the anodized surfaces probably will have somewhat lower emissivities than those used for the thermal calculations. Consequently, differences in the emissivities between thermal and straylight calculations are on purpose

4.5 Dimensions used

The most important dimensions as used in the ASAP model are shown in the following table:

Item	Dimensions (mm)
radius of small scattercone	16.5
Z-distance of sunshade	1844 - 12 for MLI = 1832
cylinderbaffle radius	250
cylinderbaffle height (in X)	141
width (in X) of gap between cylinder- and conebaffle	12 worst case, 5 best case
conebaffle upper radius	250
conebaffle lower radius	180.8
conebaffle height (in X)	454.9
CVV height (in X)	21
width (in X) of gap between CVV and thermal shield 2 baffle	14.5 in orbit, including 0.5 margin
minimum inner radius of CVV	144
inner radius thermal shield 2 baffle	145
height (in X) of thermal shield 2 baffle	118
minimum inner radius of instrument shield baffle cylinder	154
distance between thermal shield 2 baffle lower edge and instrument shield flat	10

The dimensions given are valid for ambient conditions, these dimensions change slightly for the real temperatures (programmed within ASAP)

The lower end of the cylinder/cone baffle is 10 mm above the CVV plate. The large width of the gap between CVV and heat shield 2 is determined by the situation on ground (vibration clearance under ambient pressure required).

4.6 Emissivities and Temperatures used

a) pessimistic case

The emissivities and temperatures used for the nominal case are listed in table 6.4-1 in connection with the results.

The following remarks are important to note:

Sunshade temperature: According to latest information, the worst case temperatures (EOL, hot case) will be for the central panel 200 K, + 14 K uncertainty, and for the side panels 180 K, + 14 K uncertainty. As we did not distinguish between central panel and side panels in our calculations, we here inserted an average worst case temperature of 204 K.

One should emphasize that this is a worst case temperature EOL. Most of the observing time, including hot case BOL will exhibit much lower temperature.

Emissivities of most objects are rough estimates only. They are based on worst case assumptions up to now, not on real measurements.

The emissivity of the gap between sunshade and M1 turned out to be an important factor, it was assumed to be 0.9 in issue 2. Therefore the effective emissivity of this gap was calculated in detail in a separate calculation (see chapter 5.3). It turned out to be only about 0.08. In order to account for some uncertainties, this was raised to 0.10%

The effective temperature of the gap between CVV and Thermal Shield 2 Baffle is not determined by the average temperature of these two items. Instead it is determined by the average of the temperature of the CVV and the temperature of the outer MLI sheet on top of Thermal Shield 3. This latter temperature is nearly the same as the temperature of the CVV. Therefore the effective temperature of this gap was set to the same temperature as the CVV.

b) optimistic case

The emissivities and temperatures used for the optimistic case are listed in table 6.4-2 in connection with the results.

5 Supplementary Calculations

5.1 Obscuration Calculations

The obscuration effect on throughput for the different versions of the scattercone and the legs is cited from a calculation in RD1:

obscuration ratios	rectangular legs	elliptical legs
small scattercone	7.7%	8.7%
large scattercone	10.3%	11.3%

The obscuration effect on resolution is given in figures 5.1-1 through 5.1-3. The ascending curves represent the encircled energy in percent. The curve for the unobscured pupil (figure 5-1) is given as test for the ASAP routine used for the calculation. The ASAP result is 86% encircled energy at the first dark ring while the theoretical value is 83%; this excess is an artefact of the generation of the figure, i.e. a peculiarity of ASAP. Thus the following figures should be regarded keeping in mind that the values of ASAP are too high by about 3%.

The values for the small and large scattercone are 82% and 78% encircled energy at the first dark ring (figures 5.1-2 and 5.1-3).

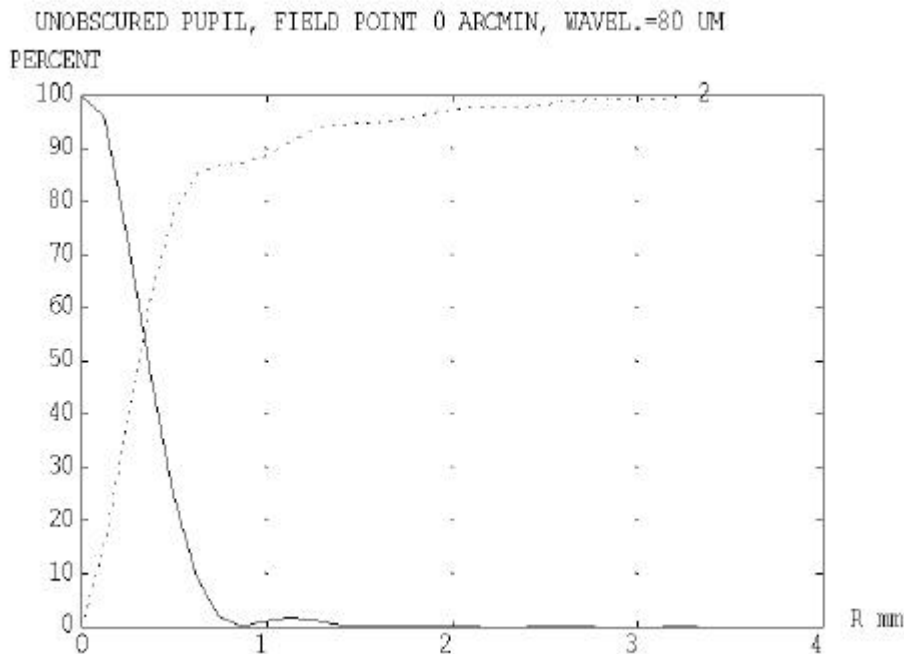


Figure 5.1-1: Radial energy distribution and encircled energy for an unobscured pupil.

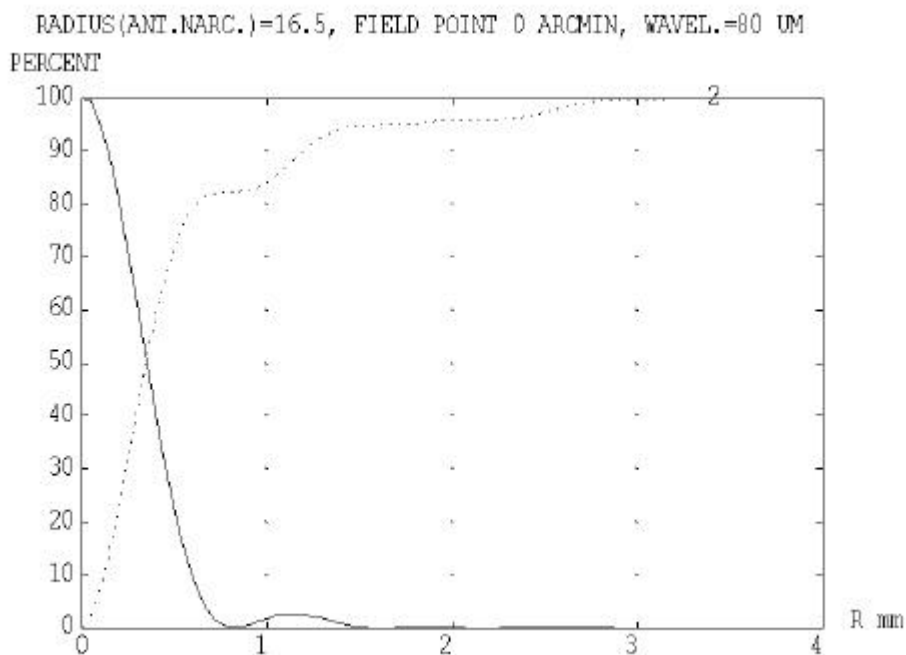


Figure 5.1-2: Radial energy distribution and encircled energy for an obscuration with a scattercone with radius 16.5 mm.

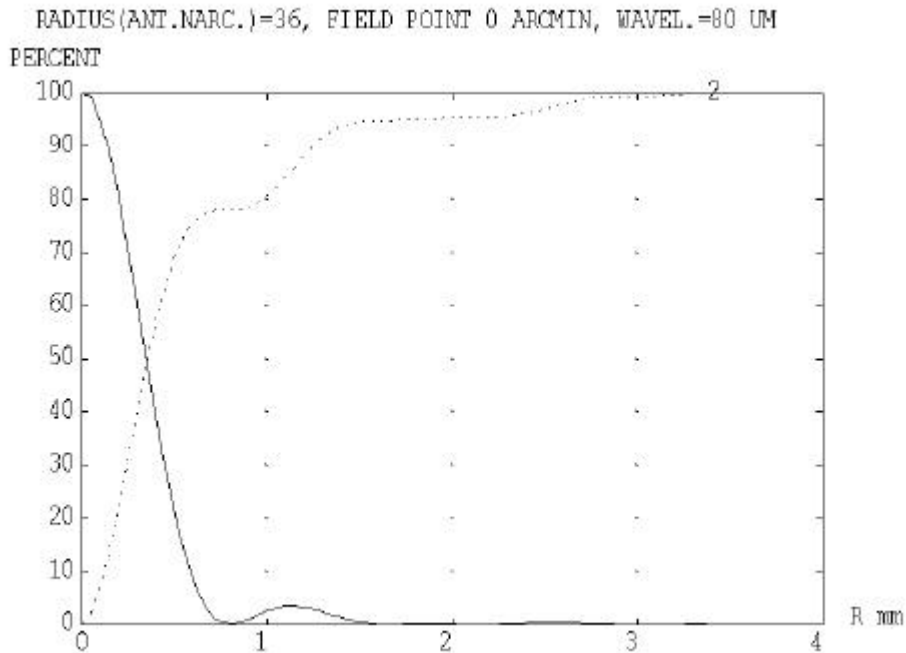


Figure 5.1-3: Radial energy distribution and encircled energy for an obscuration with a scattercone with radius 36 mm.

5.2 Straylight from LOU windows via multiple reflections within the Thermal Shields

Straylight can enter the instruments also from the warm LOU windows via multiple reflections between the individual thermal shields. One finds:

- 1) path towards the slit between CVV and Thermal Shield 2 Baffle
- 2) path towards the slit between Thermal Shield 2 Baffle and Instrument Shield Baffle.
- 3) path is oscillating between the Instrument Shield and the instruments itself towards the slit between Instrument Shield Baffle and Instruments,

(these paths continue towards the instruments finally).

Description of calculations

For reasons of ray statistics, these specific paths were calculated towards the following targets only:

- 1) gap between CVV and Thermal Shield 2 Baffle (Tube with 14 mm height x 145 mm radius)
- 2) gap between Thermal Shield 2 Baffle and Instrument Shield Baffle (Ring with outer radius of 154 mm and inner radius of 145 mm)
- 3) gap between Instrument Shield Baffle and Instruments (approximated only by a Tube with about 155 mm height x 154 mm radius)

A separate ASAP model was programmed for this case.

The overall view is shown in Figure 5.2-1

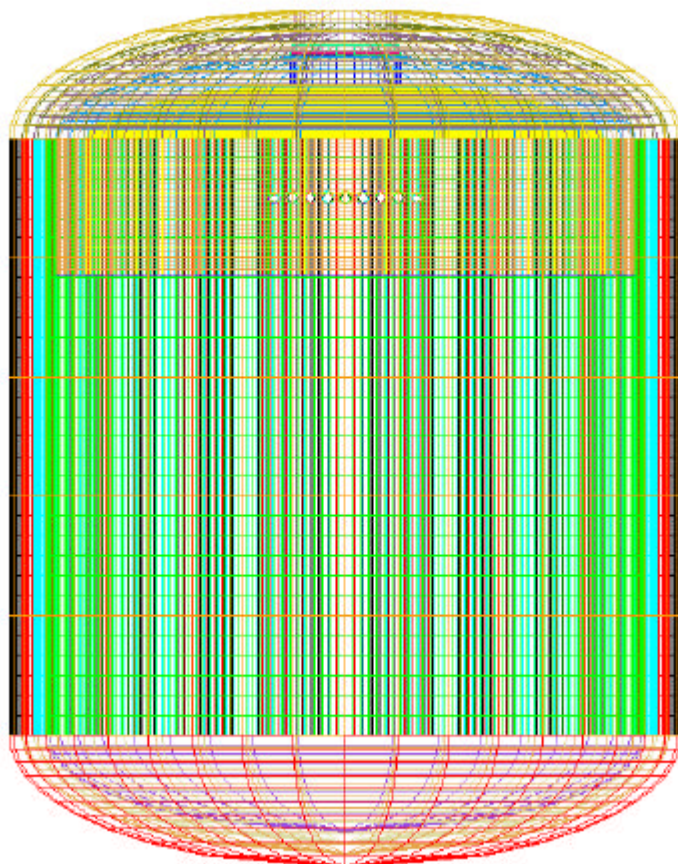


Figure 5.2-1: Overall view of the separate ASAP model.

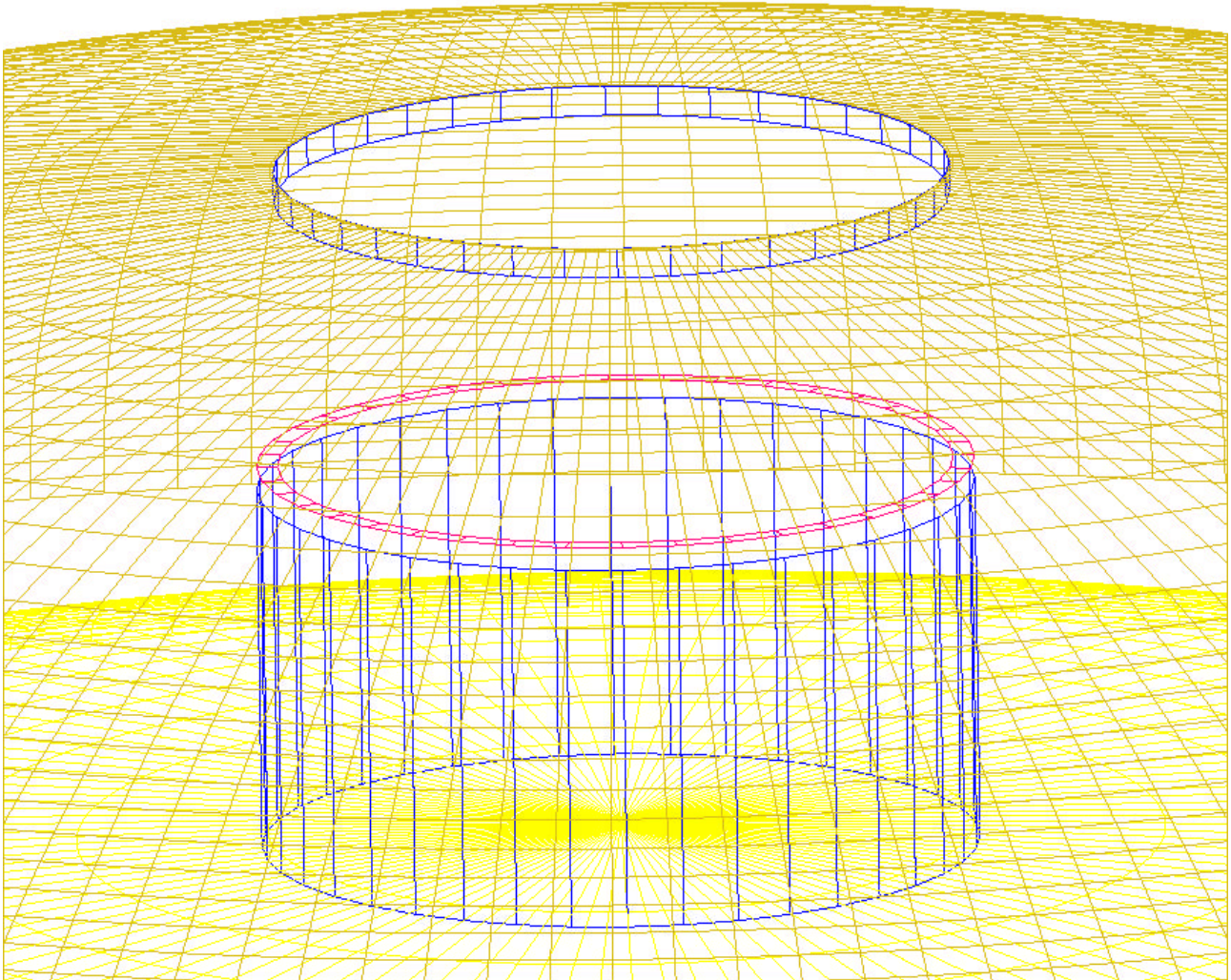


Fig.5.2-2: Detail showing the CVV top sphere, the instruments represented by the lower sphere, and the three target areas in between

The further calculation from these various gaps towards the instrument detectors then is done by the usual raytrace (with the large main ASAP model) by inserting the output from this raytrace as a source.

The rays coming out of LOU were emitted into the half sphere. Figure 5.2-3 shows the location of the emitting surfaces.

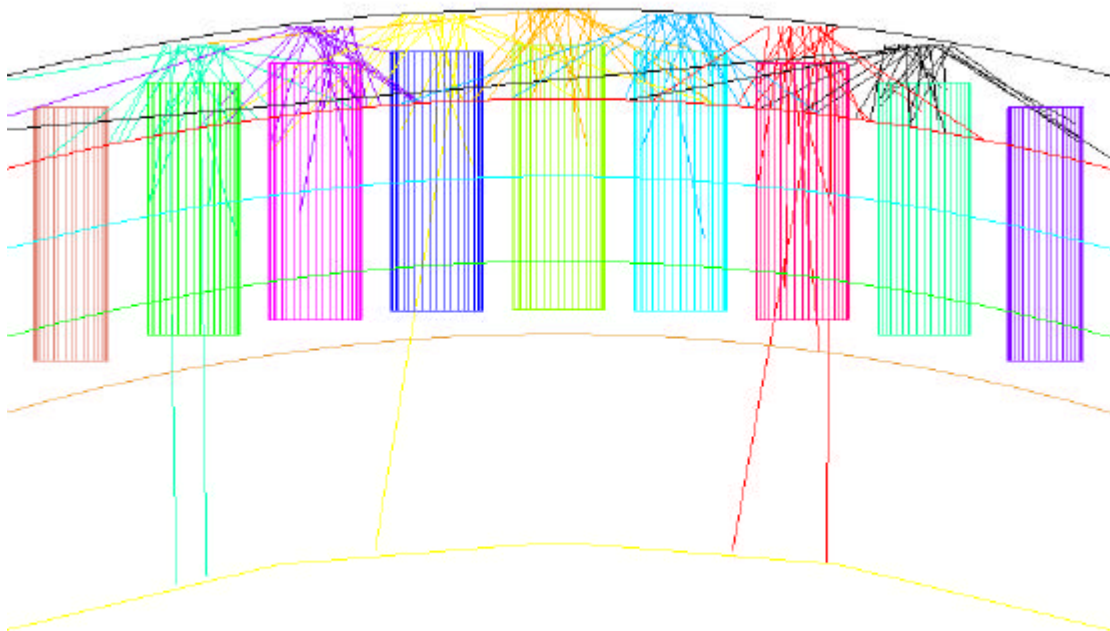


Fig. 5.2-3: Detail showing the location of the sources in relation to CVV and baffle tubes. The different spheres from top to bottom are CVV, Thermal Shields 3, 2, 1, Instrument Shield and Instruments

No scattered rays were calculated. However, in order to simulate some minor ray deviations, a roughness random parameter of size 0.02 radian was introduced (for tubes and top spheres only, not for bottom spheres and for LOU baffles), which slightly changes the ray direction from pure specular after each reflection on these surfaces. Otherwise every ray will end up on its own path around the system and never can reach a target if it has the wrong initial direction, even if it is reflected 10 000 times. The rationale for this also is that we have MLI on the Thermal Shields which have deviations at least in that order.

Intermediate results

Results have been produced for 2 different cases:

- a worst case calculation with
 - An extreme reflectivity of 0.999 of the CVV, the Thermal Shields and the Instrument Shield.
 - The maximum number of reflections per ray is 10 000.
 - The Instrument reflectivity is 0.95 (non-polished surfaces, with many edges in reality).
 - The reflectivity of the LOU baffle tubes was selected to be 0.8 instead of 0.3 (as for thermal calculations) for the following reasons: The thermal coefficient of $e=0.7$ (=reflectivity 0.3) is for shorter wavelengths in the order of 10 microns rather than the wavelengths to be considered here. Usually reflectivity goes up, when the wavelength goes up. Also in reality the reduced reflectivity is for the inner side of the tubes only, whereas in the model there is only one reflectivity for inner and outer side.
- a probable case calculation with
 - A more moderate reflectivity of 0.995 of the CVV, the Thermal Shields and the Instrument Shield.
 - The maximum number of reflections per ray is 2 000.
 - The other parameters (reflectivity of baffle tubes and instruments) are the same as for the worst case calculation.

The 7 holes of the LOU windows (with 34 mm diameter each) have a total area of 6355 mm². The ASAP flux emitted from this area into all directions therefore was 6355 (since the standard irradiance of ASAP is 1.0 in our case). It is important to note, that the irradiance at begin into all directions in the normal ASAP calculation with the large main ASAP model (from the targets towards the instruments) is 1.0 too.

The ASAP flux on the targets are

- worst case
 - 383 on target 1 between CVV and Heat Shield 2 Baffle)
 - 28 on target 2 between Heat Shield 2 Baffle and Instrument Shield Baffle
 - 271 on target 3 between Instrument Shield Baffle and Instruments
- probable case.
 - 153 on target 1 between CVV and Heat Shield 2 Baffle
 - 8 on target 2 between Heat Shield 2 Baffle and Instrument Shield Baffle
 - 243 on target 3 between Instrument Shield Baffle and Instruments

By selecting the worst case, this means that we have to finish the calculation towards the instrument detectors with a temperature of 150 K and the following fluxes from these targets:

- Target 1: flux from 383 mm² area
- Target 2: flux from 28 mm² area
- Target 3: flux from 271 mm² area

These intermediate results for the worst case are treated further in chapter 6.4

5.3 Calculation of an effective Emissivity for the Gap between Sunshade and M1

In the former issue 2 of this TN, the straylight via the gap between sunshade and M1 was approximated by a worst case assumption. The radiation coming from the S/C structure (part of sunshade below M1 rim, sunshield, CVV outer surfaces etc.) via this gap towards M2 was approximated by the radiation of a black surface (emissivity 0.9) between sunshade and M1, with the maximum temperature of the sunshade. Mainly due to diffraction at the M2 rim, this intense radiation would cause a quite high contribution to the straylight. For this reason, the effective emissivity was analysed with specialised ASAP models.

Model description

a) Extended Model

A separate ASAP file was created, which mainly consists of

- a target in the vicinity of M2
- the sunshade. In this model, it is subdivided into an upper and lower part. The lower part comprises the lower sunshade rim up to the X coordinate of the M1 rim. It emits with a worst case temperature of 204 K. The upper part is not emitting, because only the emission via the gap between sunshade and M1 is calculated here. It only reflects radiation.
- the sunshield. It emits with a worst case temperature of 273 K.
- stiffeners at sunshade and sunshield (1 for sunshade, with the temperature of the sunshade and 2 for sunshield, with the temperature of the sunshield). They emit into both directions.
- the M1 upper and lower surfaces. The lower M1 surface emits with a temperature of 139 K (worst case temperature of the MLI outer facesheet on M1).
- the M1 baffle and CVV cavity. Its outer surfaces emit with a worst case temperature of 127 K.
- The CVV. The upper spherical part of the CVV cavity emits with a worst case temperature of 144 K. The lower spherical part and the cylindrical part of the CVV cavity emit with a worst case temperature of 165 K.
- Radiation shields on + and - Y sides of the CVV cylindrical part. Its surfaces emit with a worst case temperature of 148 K into both directions.
- A radiation shield on -X, -Z side of the CVV. Its upper surface emits with a worst case temperature of 120 K and its lower surface emits with a worst case temperature of 141 K
- The Service Module. It emits into +X half sphere with a worst case temperature of 245 K
- Struts between Sunshade/Sunshield and CVV: The 12 struts are approximated by only 2 struts with 6-fold diameter, in order to represent the correct overall surface size. The temperatures of these struts have been assumed to be 200 K (no information available, because they are not represented in the thermal model).

The selected emissivity for all these surfaces was 0.05. The overall design can be seen in figures 5.3-1 and 5.3-2. As these calculations have been performed already end of 2002, the some minor deviations of the configuration occurred since then. Especially the upper form of the sunshade and the length of the CVV have changed in the meantime. However, the impacts onto these specific calculation results will be marginal.

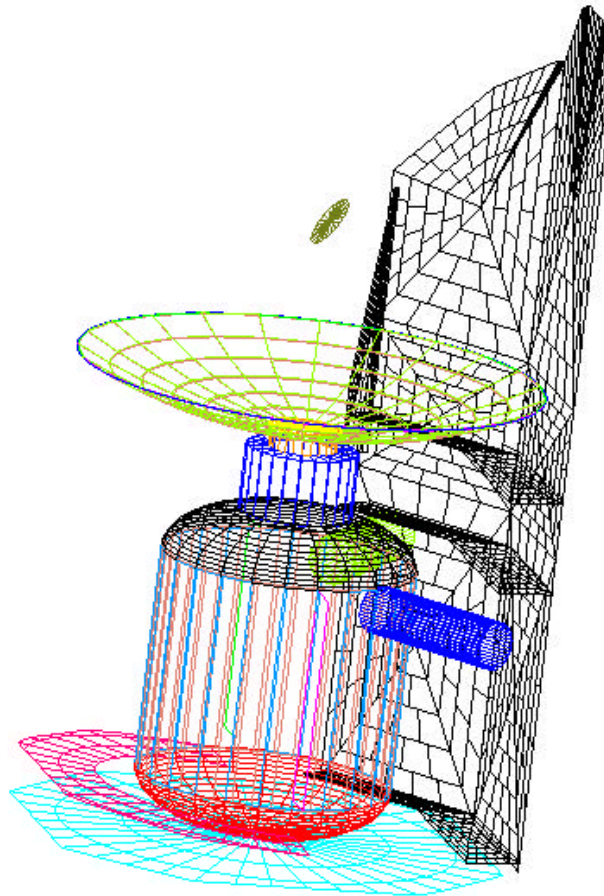


Fig. 5.3-1: Overall view of the Extended Model. For better visibility of some structures, the right part of the sunshade is not shown in the picture.
The small circle above M1 is the target surface for all calculations. This target surface is placed at the location of M2.

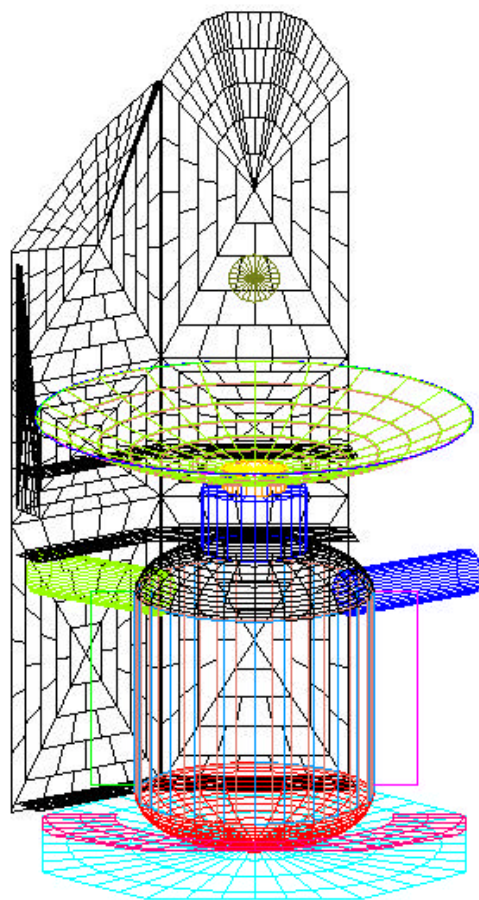


Fig. 5.3-2: Overall view of the Extended Model. For better visibility of some structures, the right part of the sunshade is not shown in the picture.

b) Gap Closure Model.

The Gap Closure Model shall investigate the improvement to be expected from an optional additive mechanical structural element. The intention of this additional surface is to significantly suppress the radiation from the surfaces below.

An additional surface was introduced between the sunshade and M1, 10 mm below the -X edge of the outerM1 rim (see Fig. 5.3-3 through 5.3-5). The Y and Z limits follow the M1 outer rim on -Z side and the sunshade on +Z side. This additional surface also emits into both directions with the worst case temperature of the sunshade of 204 K. The emissivity of this surface also is 0.05.



Fig. 5.3-3: Detailed view of the section between M1 (M1 rim shown on the left side) and sunshade, for the Gap Closure Model. Only the lower part of the central sunshade is shown (vertical line on right side).

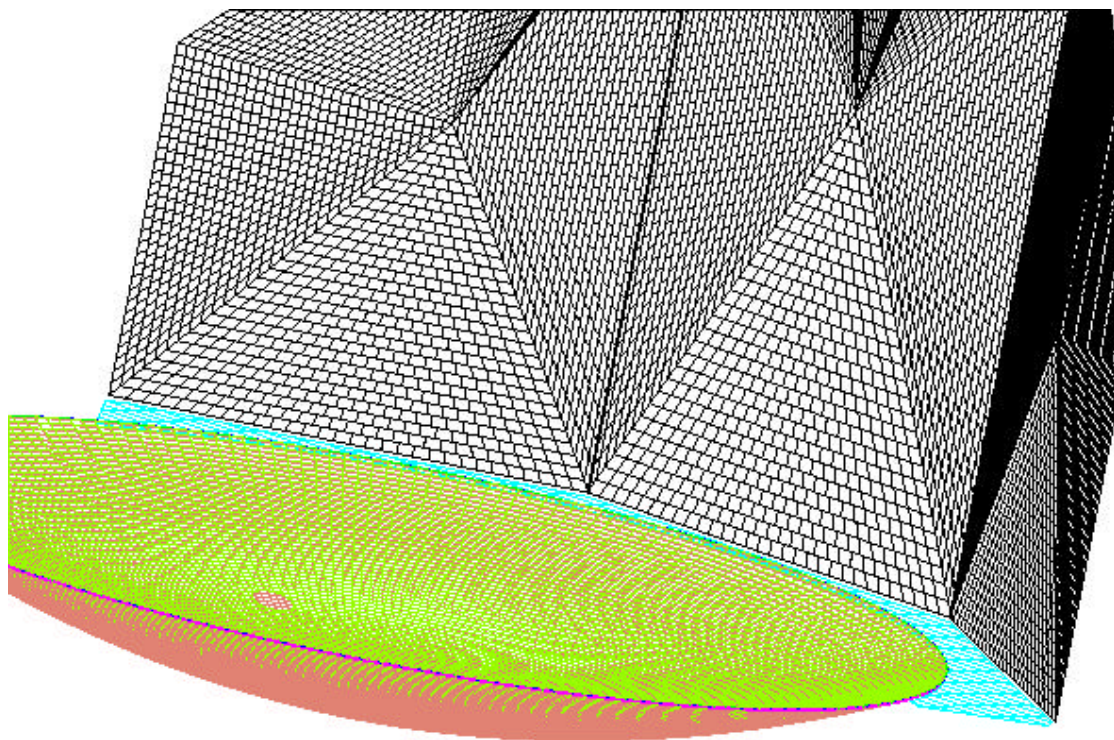


Fig. 5.3-4: Oblique view of the Gap Closure Model. For better visibility, surfaces below the gap and M1 are not shown.

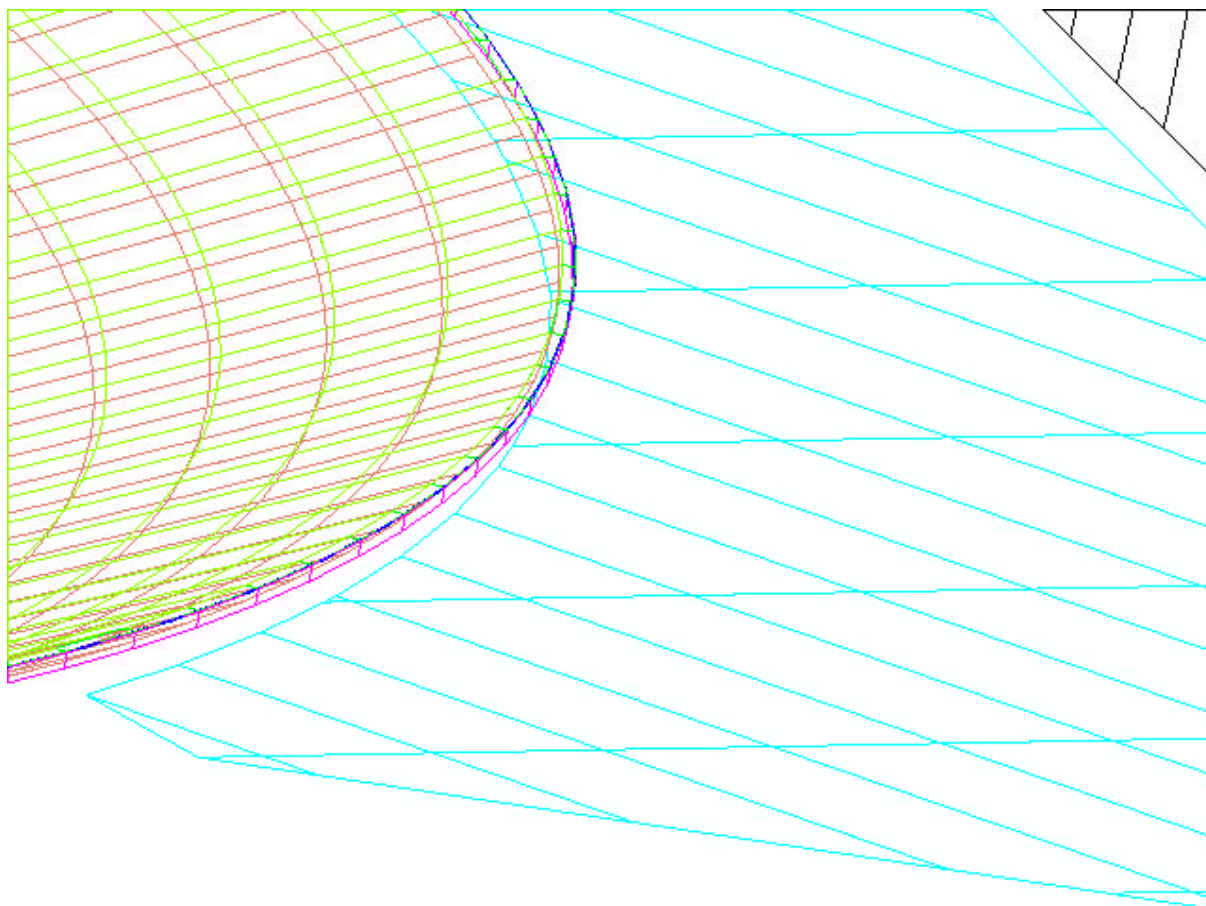


Fig. 5.3-5: Detailed oblique view of the section between M1 (M1 rim shown on the left side) and sunshade, for the Gap Closure Model.

c) Comparative model

The purpose of the Comparative Model is to compare the results gained with the designs of Extended Model and Gap Closure Model with the results gained in the previous standard ASAP calculations for the gap between sunshade and M1.



Fig. 5.3-6: Detailed view of the section between M1 (M1 rim shown on the left side) and sunshade for the Comparative Model with emitting surface between sunshade and M1. Only the lower part of the central sunshade is shown (vertical line on right side).

The Extended Model and the Gap Closure Model contain a target surface at the vicinity of M2 (see e.g. Fig. 5.3-1), since there the additional straylight transport continues (diffraction, scatter). Our Comparative Model also contains this target. In addition it contains the simple apparent surface between M1 rim and Sunshade representing the gap in the normal analyses (chapter 6.4). The Comparative Model uses exactly the same temperature (204 K) and emissivity (0.9) as used in the former issue 2 of this TN. Therefore, by comparing the fluxes at the target surface near M2 of the Extended Model with the Comparative Model we see whether the assumptions on temperature and emissivity for the gap surface between the M1 rim and Sunshade in the usual analyses of chapter 6.4 have to be corrected.

By comparing the Gap Closure Model with the Comparative Model we in fact have a comparison with the Extended Model. So the benefit of the gap closure can be deduced.

Intermediate results

Results have been gained for 3 different wavelenghts, 80, 230 and 670 μm . They are as follows (arbitrary ASAP units):

	80 μm	230 μm	670 μm
Extended Model:	4087	2012	1633
Gap Closure Model	3309	1582	1270
Comparative model:	44342	21106	16919

Table 5.3-1: Radiation on target for different models and different wavelenghts (arbitrary units)

The Comparative Model was with emissivity 0.9 and temperature 204°K. Therefore the corrected emissivities are (if we assume the same temperature of 204°K):

	80 μm	230 μm	670 μm
Extended Model:	0.0830	0.0858	0.0867
Gap Closure Model	0.0672	0.0675	0.0676
Comparative model:	0.9	0.9	0.9

Table 5.3-2: Real emissivities of the gap between sunshade and M1, 204 K assumed.

The results show that the emission from the gap between sunshade and M1 is much lower than assumed in the former issue 2 of this TN. The emissivity for the extended model is in the range of 0.083 - 0.087 instead of 0.9. Due to the simplifications in the model there might be an error in the range of 10 %. **The emissivity of the gap between sunshade and M1 in chapter 6.4 therefore is set to 0.1, at a temperature of 204 K**, because from the values gained it seems not necessary to correct the effective temperature of the gap. The results further show, that there will be no large gain by the introduction of a low emitting foil at Sunshade temperature between Sunshade and M1 (difference between Extended Model results and Gap Closure Model results). The mechanical effort and risk (vibration) are too high for that moderate gain.

6 Thermal emission (Self emission)

6.1 Introduction

For most of the emitting objects, the purely specular paths are the dominant ones. The standard raytrace commands of ASAP have been used for the calculations.

The scattering functions mentioned in the appendix (chapter 11) have been used for those cases where scattering is important (mirrors, filters). The scattering calculations require the definition of a solid angle into which the scattering occurs. For reasons of disk storage and calculational speed, this solid angle is limited as found necessary.

There are no standard ASAP commands available for all cases of diffraction. Therefore the diffraction is calculated separately, see section 6.2. Also the case of thermal emission from the HIFI oscillator window requires some explanation, see section 6.3.

6.2 Diffraction Calculations

6.2.1 Introduction

Three methods are used for the diffraction calculations

- method of stationary phase
- method with Fresnel-Integrals (after Born&Wolf, only for comparison).
- ASAP's coherent field synthesis

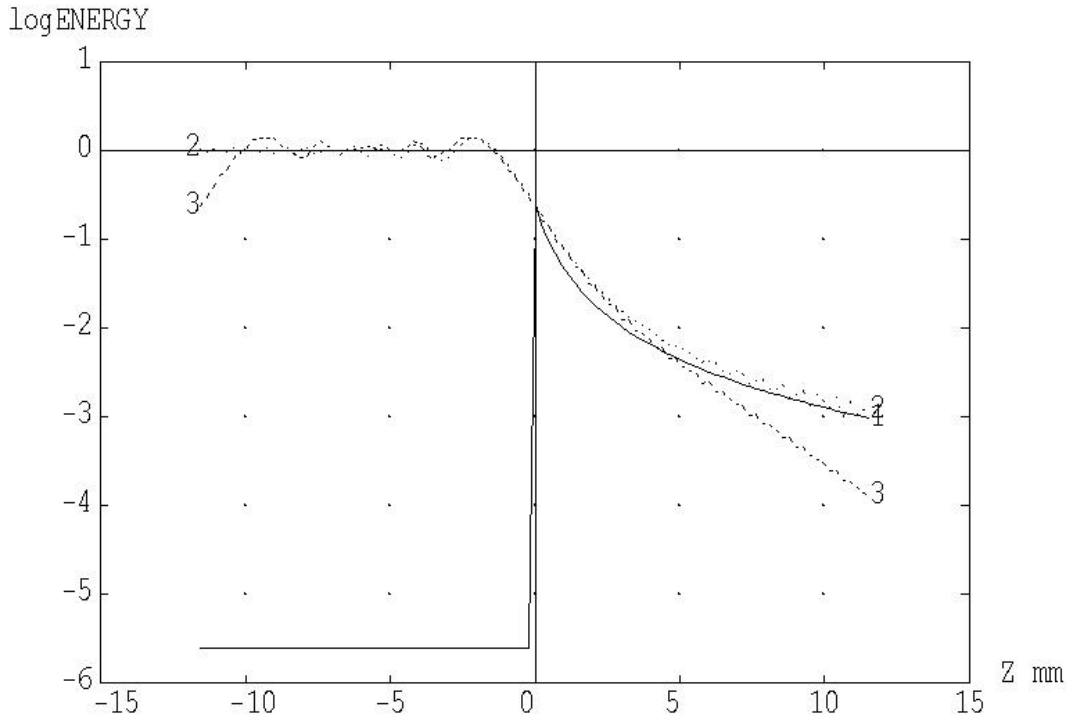
The coincidence of two or three methods gives confidence that the numerous radiometric multiplications with solid angles, areas of emitting/receiving surfaces etc. are correct.

The method of stationary phase is fairly general in application. The results are correct even for large angles of diffraction; very close (roughly < 1 degree) to the shadow limit the results tend to approach infinity and must be clipped.

The method with Fresnel-Integrals is restricted to simple cases (at least in the example worked out in Born&Wolf), therefore it is used only as a check in order to verify the results of the other two methods.

ASAP's coherent field synthesis may be applied for geometries where a coherent wavefront can be traced across the objects in question without disturbing the following field synthesis of ASAP. The method is less accurate, if large diffraction angles occur.

IRRADIANCE 57.28996 MM BEHIND A SCREEN WITH STRAIGHT EDGE



WAVELENGTH .1 MM. ABSCISSA: 1 MM = 1 DEGREE DIFFRACTION ANGLE.
 CALCULATION DONE WITH: METHOD OF STATIONARY PHASE (CURVE 1),
 FRESNEL INTEGRALS (CURVE 2), ASAP'S COHERENT FIELD SYNTHESIS (CURVE 3)

Figure 6.2.1-1: Diffraction behind a straight edge calculated by three methods (wavelength is 0.1 mm).

These properties can be seen in figure 6.2.1-1, i.e. a simple case selected only for the purpose of comparison. The irradiation impinging on a screen with straight edge is a plane wave (i.e. the source is at infinity). The intercepting plane is 57 mm behind the screen. On the left side there is the illuminated half while the shadow is on the right side. Near the shadow limit the linear dimension in mm coincides with degrees of diffraction angle (it is proportional to the tangent of the diffraction angle). The logarithm(10) of the relative irradiance is plotted as obtained with the three methods. The line for the method of stationary phase has not been calculated in the illuminated region (therefore drops to quasi zero).

The cases treated/mentioned in the next chapters are

- diffraction at the rim of apertures in the telescope focal surface
- thermal emission from the gap of the sunshade diffracted into the field of view by the rim of the secondary mirror.

The case with the secondary mirror as diffracting edge is a special case, since this diffracting edge can be seen by the detectors; it is imaged onto the rim of the cold stops / chopper elements probably without any appreciable clipping. Thus a single diffraction at the rim of the secondary is sufficient to redirect radiation onto the detectors. The case with the gap around the cryocover (and other similar cases) is different, at least another scattering/diffracting process is required before the diffracted rays enter the field of view. The reason for that is that all candidates for diffracting edges

- either cannot be seen by the detectors directly
- or are not irradiated by strong sources.

6.2.2 *Diffraction at the rim of apertures in the telescope focal surface*

The diffraction at the SPIRE opening was treated in issue 2 with a relative comparison with the specular irradiation. In the meantime, a more sophisticated calculational scheme for diffraction at the rim of apertures in the telescope focal surface has been generated for the case of ground testing. This scheme delivers diffracted irradiances on the detectors, thus is considered much superior than the treatment done in the earlier issue 2. Therefore the earlier calculation is abandoned in favour of the new one.

The new calculational scheme is described in detail in HP-2-ASED-TN-0076 issue 2. That TN contains the most stringent circumstances for that case, i.e. radiation from the warm objects around the cryocover during ground testing. No comparable warm objects are present in the orbit situation. Therefore no similar calculation is necessary here for the orbit case.

A supporting short calculation is mentioned here which compares the irradiances onto the SPIRE/PACS input surfaces

1. rays from the warm objects around the cryocover (during ground testing)
2. rays from the sunshade zigzagging down towards the instruments (in orbit).

The latter irradiance is more than a factor of 10 smaller than the first one, also emissivity and temperature of the sunshade are even more favourable than the case 1), the ground test. So the conclusion is correct that diffraction at the rim of apertures in the telescope focal surface is not important in orbit, i.e. less than 1%.

6.2.3 *Diffraction at the rim of the secondary mirror with the gap near the sunshade as thermal source*

As mentioned already, the diffracting edge of M2 can be seen by the detectors; it is imaged onto the rim of the cold stops / chopper elements probably without any appreciable clipping. Thus a single diffraction at the rim of the secondary is sufficient to redirect radiation onto the detectors. Therefore a calculation of the diffracted radiation impinging on the telescope focal surface is sufficient for a judgement of that straylight case.

ASAP's coherent field synthesis was chosen for that calculation, since it is straightforward to include the two obscuring hexapod legs into the analysis (it would be quite laborious to do the same with the stationary phase method). 29 coherent point sources are placed along the gap, they radiate towards the rim of the secondary mirror. The beams are propagated onto the telescope focal surface. There the coherent field synthesis is done separately for each source. Afterwards the irradiance of each source is added incoherently. Figure 6.2.3-1 gives an impression of the beams used for the calculation. The beams of two sources are clipped partially by two hexapod legs, so a possible diffraction effect by the legs is included. The instrument structure is not included, since the intention is to present a broader distribution of the diffracted radiation on the telescope focal surface in the graphs; the small instrument openings would include only a small fraction of the spatial distribution of the irradiance.

The radiance of the source is set to the same value as usual in our thermal calculations ($=1/\pi \cdot 1/(\text{sr} \cdot \text{mm}^2)$), so a comparison with the radiation of the telescope mirrors can be done easily. The usual correction factors for emissivity ($=0.10$) and temperature (204 K) for the gap near the sunshade are applied. The radiating gap has an area of 8520 cm². Compared to issue 2, the new effective emissivity of 0.10 (calculated in chapter 5.3) leads to a substantial reduction in the corresponding straylight value. It no longer represents a strong straylight source.

A normalization of the mirror contribution to 100% is included as usual. Thus the curves presented here are to be interpreted as in the earlier analysis: a value of 1.0 (or 0 in the log(10)-diagrams) corresponds to 1% of the thermal radiation of both telescope mirrors.

The irradiance is plotted across the Y-coordinate in figure 6.2.3-2, across the Z-coordinate in figure 6.2.3-3. The positions of PACS and SPIRE are near Z=+80 and Z=-90 mm. Both diagrams are valid for a wavelength of 0.23 mm thus touch both wavelength regions of PACS and SPIRE. The corresponding figures 6.2.3-4 and 6.2.3-5 are valid for 0.67 mm wavelength (SPIRE only), see also figures 6.2.3-6 and 6.2.3-7 for 0.08 mm wavelength (PACS only). The positions of the scans are listed in the figure subscripts.

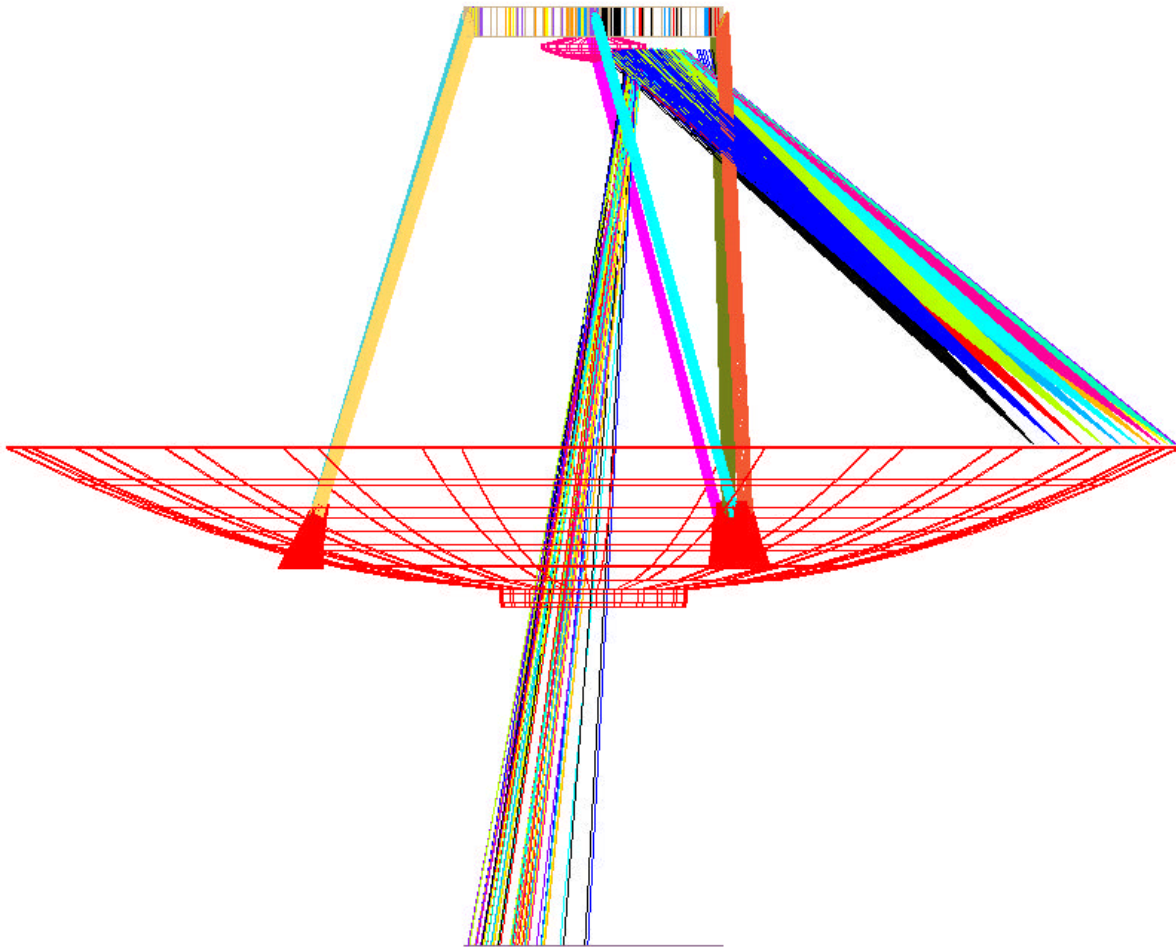


Figure 6.2.3-1: Beams used for the calculation of diffraction at the rim of the secondary mirror, source is the gap near the sunshade.

The resulting straylight is read from the figures mentioned. For SPIRE, one has to take into account that the rim of the secondary is seen with reduced sensitivity due to the edge taper of 8 dB (or 13%) introduced by the horns of SPIRE. The edge taper is not included in the figures which represent the pure diffraction variation. So the numbers for SPIRE (taken from the figures) are reduced by the factor 0.13. The results are

wavelength	0.08 mm (PACS)	0.23 mm (PACS)	0.23 mm (SPIRE)	0.67 mm (SPIRE)
irradiance	0.3%	0.5%	0.4%	1.3%

The scaling law for diffraction (proportional to wavelength) is not the only parameter influencing the diffraction curves; due to the comparison with the thermal radiation of the telescope mirrors also the variation of the Planck curves with wavelength for different temperatures counts. All the numbers describe a worst case situation with the average temperature of the sunshade set at 204 K, i.e. the thermal hot case.

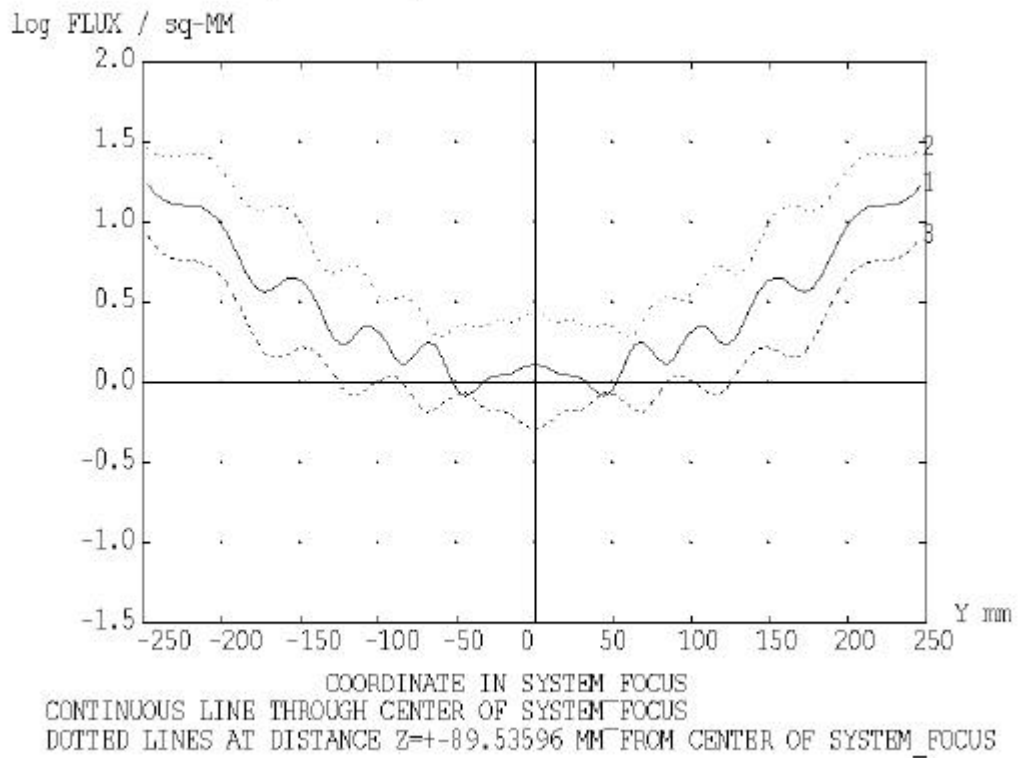


Figure 6.2.3-2: Irradiance on system focal plane with scans across Y-coordinate (wavelength 0.23 mm)

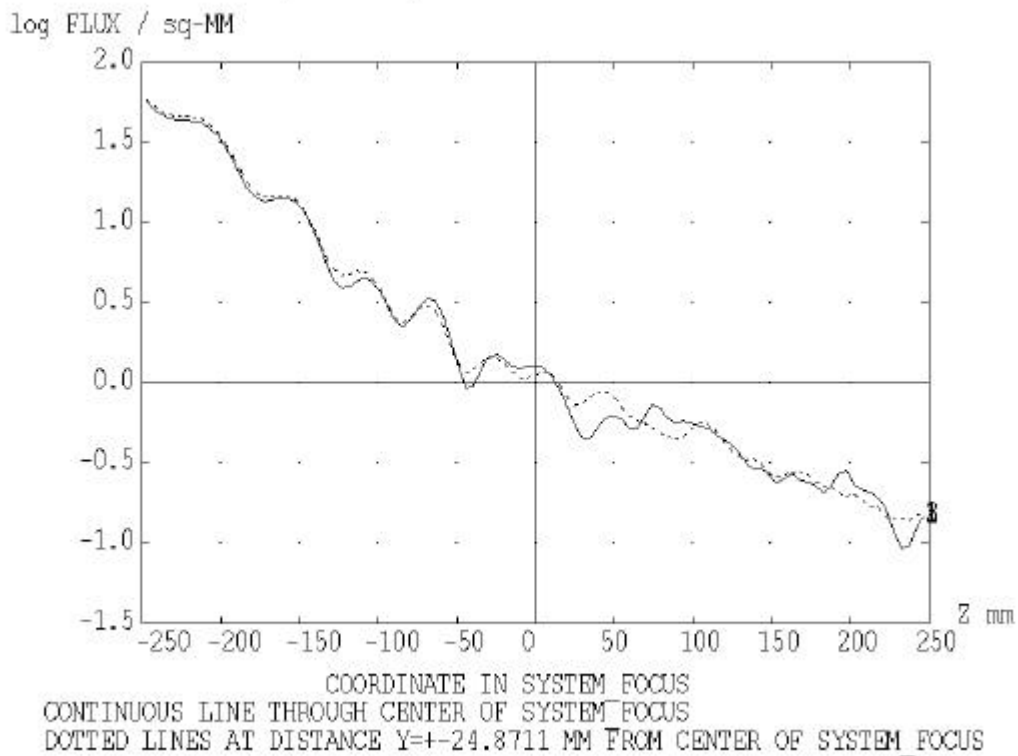


Figure 6.2.3-3: Irradiance on system focal plane with scans across Z-coordinate (wavelength 0.23 mm)

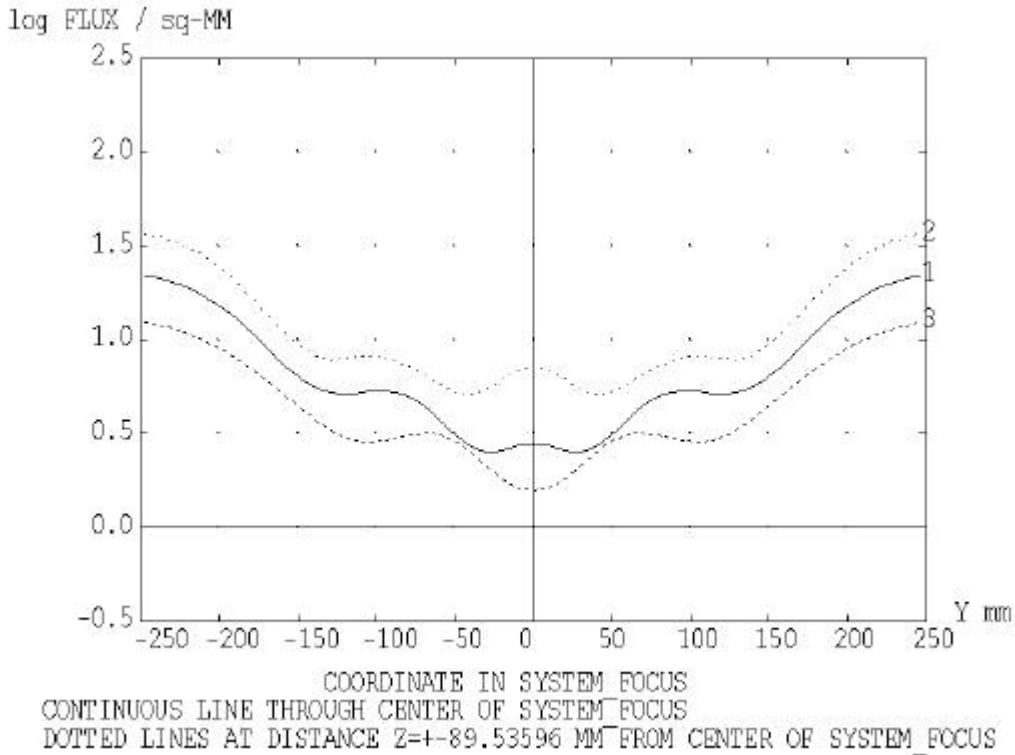


Figure 6.2.3-4: Irradiance on system focal plane with scans across Y-coordinate (wavelength 0.67 mm)

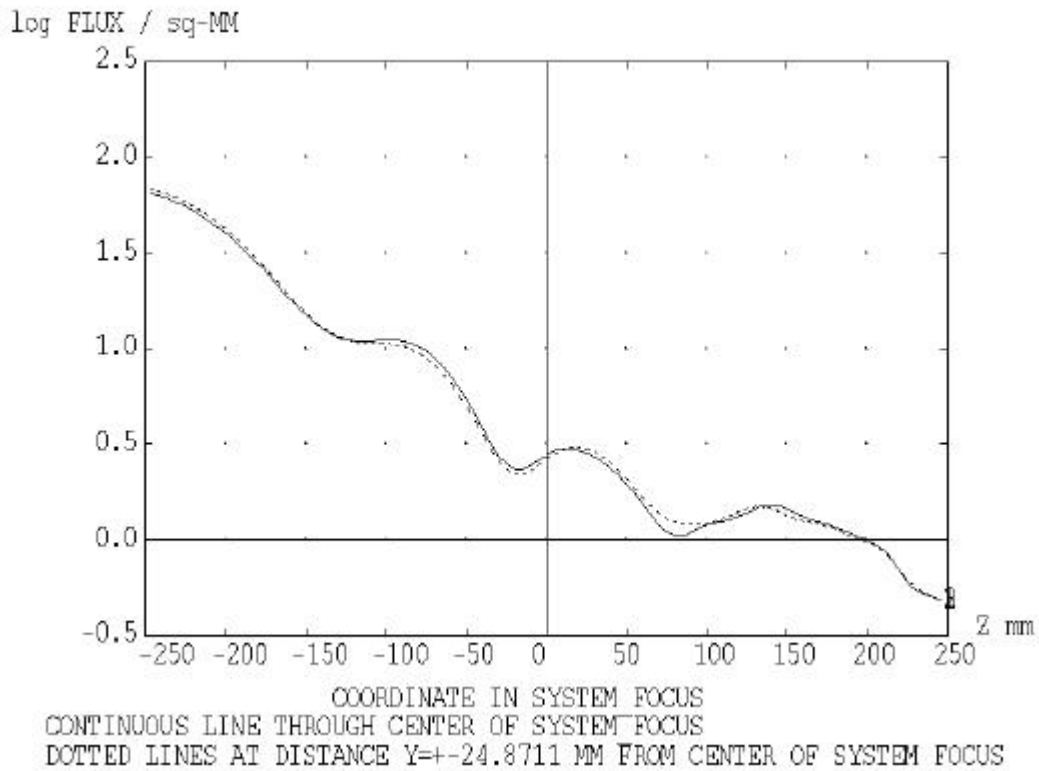


Figure 6.2.3-5: Irradiance on system focal plane with scans across Z-coordinate (wavelength 0.67 mm)

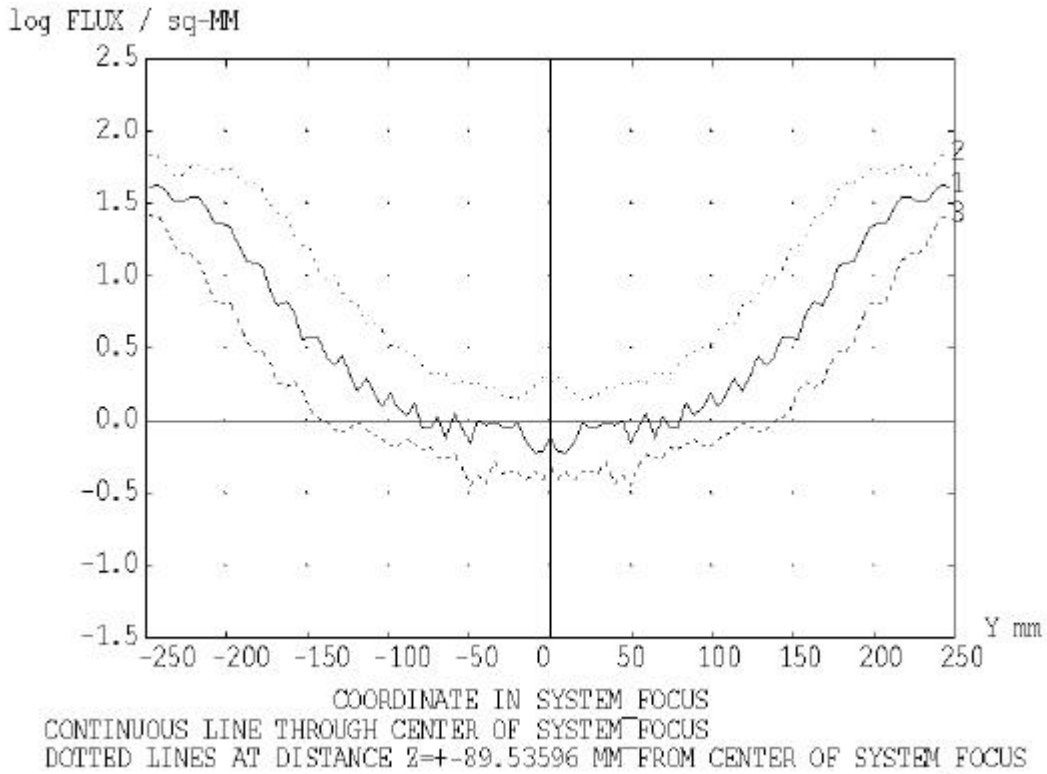


Figure 6.2.3-6: Irradiance on system focal plane with scans across Y-coordinate (wavelength 0.08 mm)

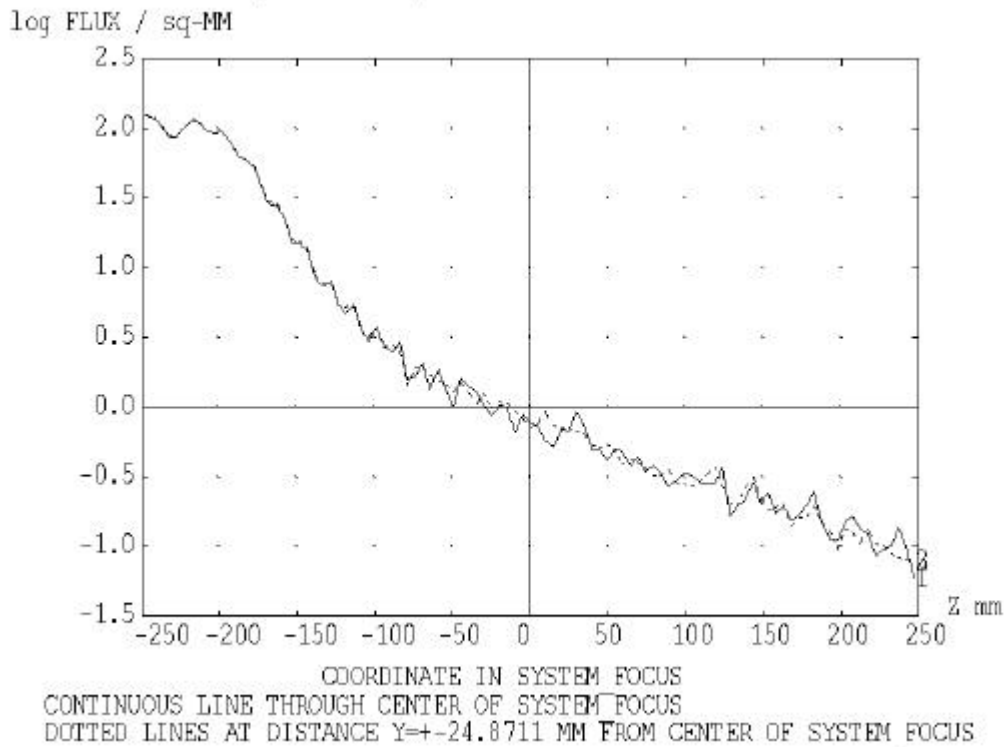


Figure 6.2.3-7: Irradiance on system focal plane with scans across Z-coordinate (wavelength 0.08 mm)

As mentioned, a complete comparison with the method of stationary phase was not programmed due to the complexity with the hexapod legs and the distribution of sources along the gap. Nevertheless, a partial comparison has been worked out by setting only a single source in the gap at $Y=0$. For that case (which does not represent the complete radiometric situation) a relative comparison has been programmed with the method of stationary phase. A scan across Z-coordinate at $Y=0$ in the telescope focal surface is the result shown in figures 6.2.3-8 (wavelength 0.2 mm) and 6.2.3-9 (wavelength 0.67 mm). The method of stationary phase (as applied) does not contain such a refinement in its mathematics that fringes could appear; however, the overall comparison is acceptable. At the shadow limit the curve for the stationary phase tends to infinity, therefore it has been clipped as usual (at the position of the dip which is not real).

The comparison shows that ASAP's coherent field synthesis is acceptable for the case of diffraction at the rim of the secondary of a source nearby the nominal beam. The fringes seen in figures 6.2.3-8 and 6.2.3-9 are less salient in the preceding figures, since there an incoherent superposition of several coherent sources along the gap has been calculated. The results of the coherent calculation are depend somewhat on the input parameters (number of rays etc.). Thus the accuracy of the results certainly has to be considered with caution, we think it is not better than a factor of 3..5. ASAP's coherent field synthesis obviously is approaching its limits for such calculations.

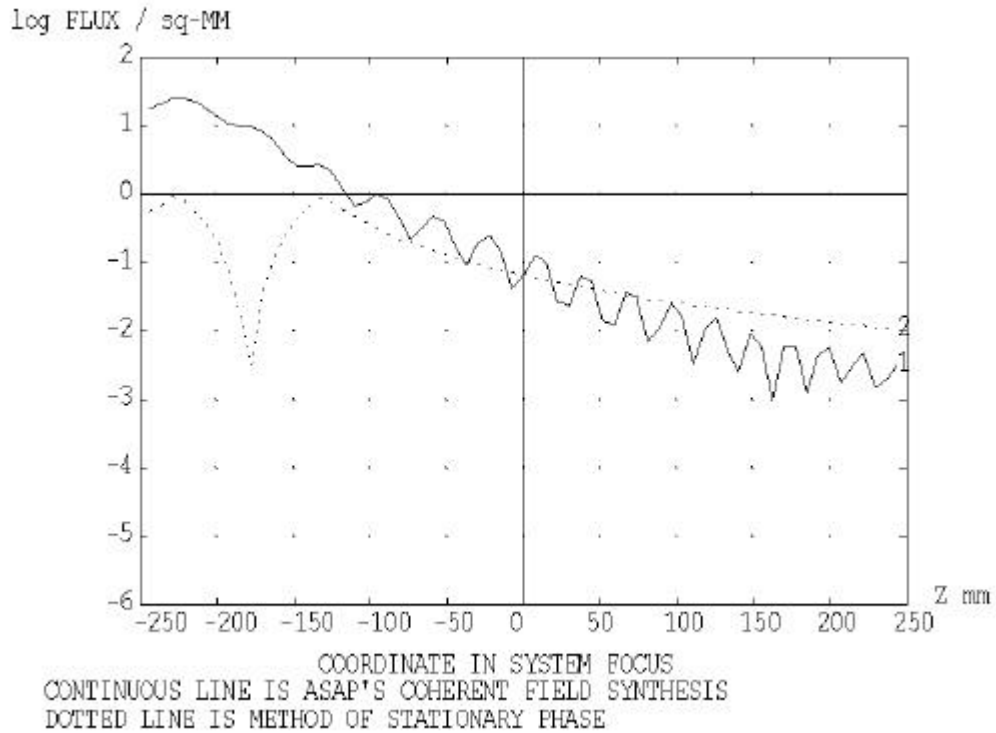


Figure 6.2.3-8: Relative comparison of two methods with a single source in the gap diffracted at the rim of the secondary mirror, wavelength = 0.2 mm

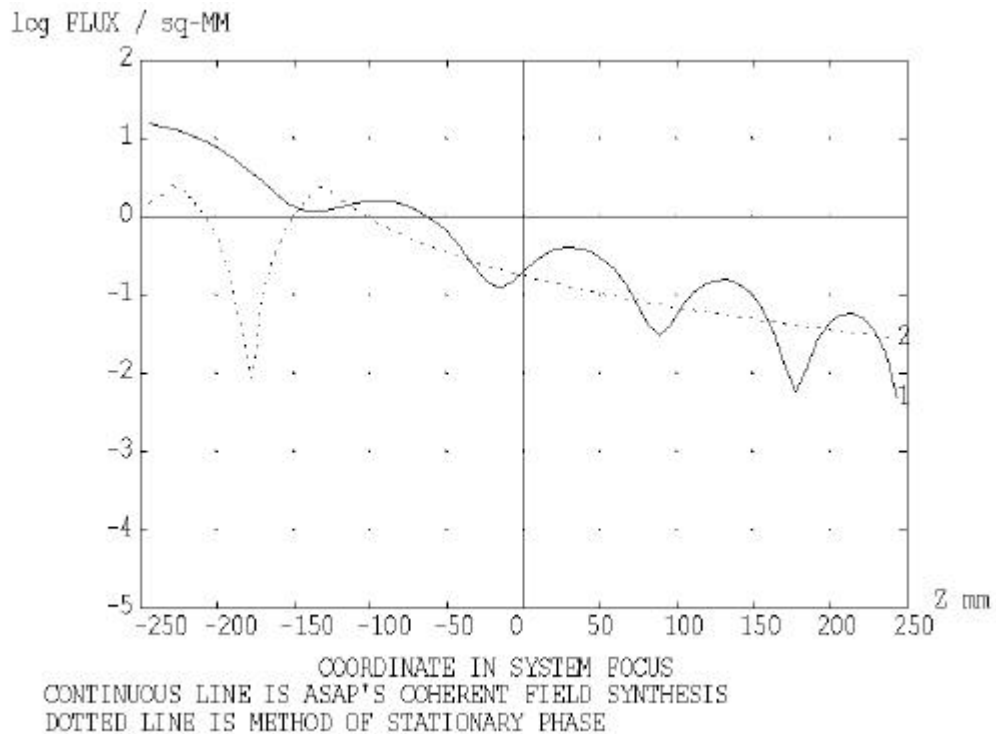


Figure 6.2.3-9: Relative comparison of two methods with a single source in the gap diffracted at the rim of the secondary mirror, wavelength = 0.67 mm

6.3 Thermal Emission from the HIFI Oscillator Window

The windows for feeding the oscillator radiation into the cold instrument region also feed in thermal radiation. We assume a black thermal radiation of temperature 150 K there with no restriction of the solid angle (i.e. hemispherical). The ASAP HIFI model contains mirrors and housing walls. The walls are quoted to have a reflectivity similar to that of mirrors, so we adopt a reflectivity of 0.99. Both the mirrors and the walls transport the thermal radiation towards the internal opening of HIFI, i.e. towards HIFI mirror M3, from there the radiation aims at +X-direction.

A first trial with a lambertian emitter at the oscillator window position with the PACS and SPIRE detectors as receiving surfaces failed, the large number of zigzag reflections within HIFI did not lead to reasonable results. Therefore the whole path was split into several steps

- a) transmission of thermal radiation through the HIFI compartments (stepwise)
- b) radiation onto PACS and SPIRE (via the M2-assembly) from a fictive thermal emitter at the HIFI opening near M3.

Step b) is described first. The black thermal radiation of temperature 150 K assumed at the oscillator window is placed at the HIFI opening near M3, the resulting radiation (via the M2-assembly) towards PACS and SPIRE clearly represents a worst case. The numbers found are 4.2% (PACS) and 5.3% (SPIRE) (with 100% as contribution of the telescope reflectors). They are not negligible, therefore it is necessary to calculate step a) too.

The transmission of thermal radiation through the HIFI compartments is calculated for

- compartment 1
- compartment 1 plus 2.

the compartment numbering is shown in figure 6.3-1.

The transmission calculations start with lambertian sources at the LOU window, the transmission is evaluated as the ratio of the fluxes out/in. The results are

Compartment	Transmission
1	0.3
1+2	0.09

The numbers depend strongly on the wall reflection assumed to be 0.99.

There are 5 compartments; the table above indicates that each compartment yields a transmission with factor 0.3, 5 compartments could give $0.3^5=0.0024$. Although only compartments 1 and 2 have been calculated, it is safe to state that the total transmission for all compartments is smaller than 0.01. So the numbers of worst case of step b) now reduces to <0.04% (PACS) and <0.05% (SPIRE). These numbers are small enough for the statement that the thermal radiation from the HIFI oscillator does not play an important role.

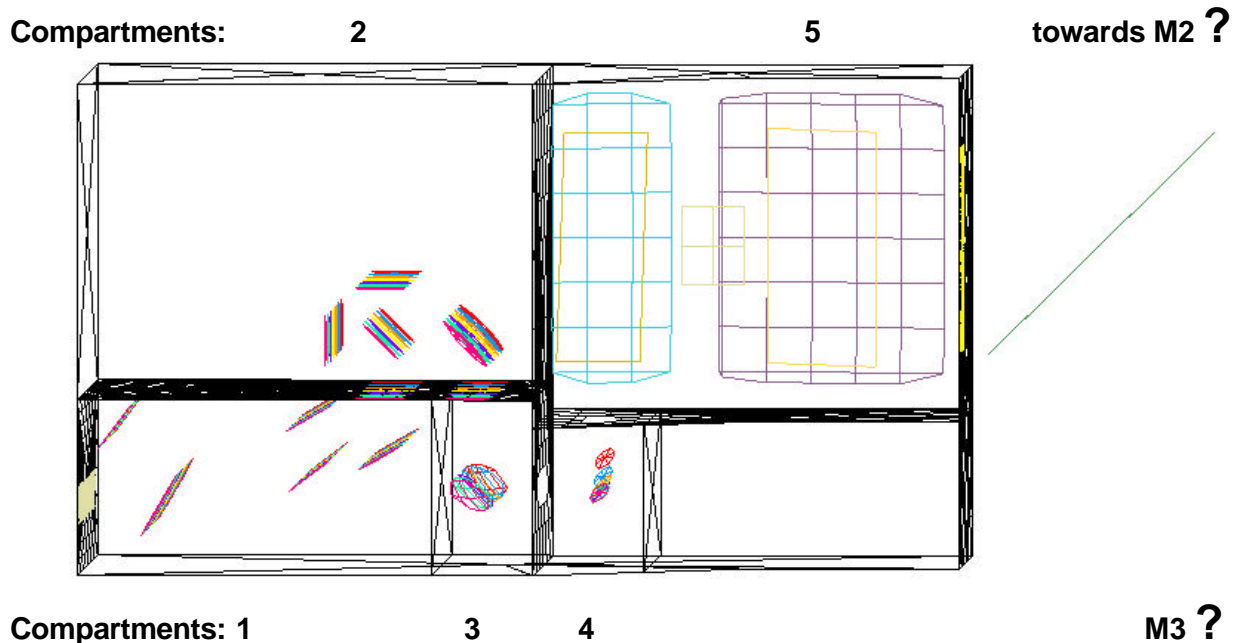


Figure 6.3-1 ASAP-HIFI model with compartment numbering. The numbers increase from the local oscillator windows (lower left side) to the inner opening towards M3 and M2 (telescope secondary mirror).

6.4 Results

Since the requirement on self emission is a number relative to the self emission of the reflectors, all calculations are done without use of a unit for flux (e.g. Watt). The emitting raygrids within ASAP all have an emitting radiance of $1/\pi$ per mm^2 per steradian. The raytrace yields a total flux value for the SPIRE/PACS detectors. The flux onto the detectors from a specific object (e.g. the sunshade) is divided by the sum of fluxes calculated for M1 and M2.

This relative flux for the specific object has to be corrected with two factors:

- Temperature correction factor: thermal emission with the temperature of the emitting object divided by thermal emission of a 70 K object (temperature for M1 and M2). This temperature correction factor depends on the wavelength.
- Emissivity correction factor: emissivity of object versus emissivity of M1 and M2.

The results are values averaged over the respective detector area.

The contribution of M1 + M2 has been set to 100 so:

- the violation of the 10% thermal emission requirement occurs if the numbers exceed 10.

The table 6.4-1 gives an overview on the expected worst case situation for the case with the rectangular cross section of the Hexapod legs and the small scattercone, as selected by the scientists. The expected temperatures of the CVV and the surrounding objects are about 75 K in the worst case, if the telescope itself is at 70 K.

For most of the emitting objects, the purely specular paths are the dominant ones. However, some paths do not follow this rule, they are marked with

- Sc = scattering, the object indication where scattering takes place is added
- D = diffraction, the object indication where diffraction takes place is added.

For the other lines, it is indicated whether the contribution is only specular or only scattered. If nothing is indicated, then it is the sum of specular and scattered (whereby specular dominates).

Table 6.4-1: Self emission onto pacs/spire detectors, pessimistic case.

Emitting object	temperature / emissivity	scattering(Sc)/ diffraction(D) on	PACS detector	SPIRE detector
Sunshade	204 K / 0.05	Sc: M1/M2, +spec.	2.326	0.611
gap between Sunshade and M1	204 K / 0.10	only Sc: M1 / M2	0.193	0.092
gap between Sunshade and M1	204 K / 0.10	only D: M2(rim)	0.5	1.3
Hexapod	70 K / 0.02		3.122	3.977
M1+M2 (without reference path)	70 K / 0.015		2.488	1.873
scattercone	70 K / 0.015		0.615	0
M1-Baffle flat	75 K / 0.05		1.382	1.098
M1-Baffle cone / cylinder	75 K / 0.05		3.537	0.499
gap (12 mm) between M1-Baffle cone and cylinder	75 K / 0.90		1.542	0.330
Cryocover mirrors	75 K / 0.05		0.676	0.025
other reflecting parts of Cryocover	75 K / 0.05		0.069	0.020
Cryocover black rim	75 K / 0.80		1.749	0.246
reflecting objects near Cryocover	75 K / 0.05		0.462	0.070
black gaps around Cryocover / M1-Baffle	75 K / 0.90		2.796	0.414
CVV top	75 K / 0.05		1.237	0.077
gap betw. CVV / Thermal Shield 2 Baffle	75 K / 0.90		0.500	0.119
Thermal Shield 2 Baffle black	43 K / 0.80	only specular	1.478	1.391
Thermal Shield 2 Baffle black	43 K / 0.80	only scattering in instrument.	0.071	0.805
Instrument Shield Baffle	12 K / 0.05		0.002	0.002
Gap below Instrument Shield Baffle	12 K / 0.90		0.076	0.033
LOU windows via HiFi	150 K / 0.90		0.05	0.04
LOU windows via heat shield gaps	150 K / 0.90		0.231	0.020
Holes in OB for cooling straps (worst case consideration only)	34 K / 0.90		0.2	0.02
sum			25.3	13.1

Data for PACS and SPIRE are in % with 100% = telescope irradiation (70 K, total $\epsilon=0.03$)

There are some positions in the tables which cause significant differences compared to issue 2.

Telescope

The BRDF for the telescope mirrors has changed significantly. The same BRDF also was used for other parts outside the CVV and therefore exposed to ambient/contamination conditions.

The contributions from the hexapod structure and the side paths via M1/M2 are different from those in issue 2, there the values from RD1 have been cited. For the present issue, those straylight contributions are based on new calculations in order to allow for

- the geometry changes of the hexapod (inclinations of the lower barrel surfaces)
- SPIRE and PACS are represented with their actual location near the telescope system focus
- SPIRE is represented with the edge taper (apodization) of the detector horns and the central blockage of its pupil.

The contributions involving the emission from M1 and M2 via side paths in table 6.4-1 are influenced by the details mentioned above. On the other hand, the emission from the scattercone remained unchanged for PACS (as it should), for SPIRE the central pupil blockage is important.

The emission from the hexapod for spire is larger in table 6.4-1 than for PACS. This is due to the fact that the emission from M1+M2 (on the reference path, used for normalization) is influenced by the SPIRE edge taper while only a marginal influence exists for the emission from the hexapod (inner part of the pupil, not the very centre).

Comparison SPIRE-PACS

Some differences between SPIRE and PACS are due to their different location in the focal region of the telescope. But more important is the fact that the ASAP model of SPIRE has a central blockage of the pupil. Whether this blockage in reality will be as good as in the ASAP model, depends on problems of misalignment etc. Thus the values for SPIRE in some cases could come closer to those of PACS in case of misalignment. Nevertheless, some differences will always be present due to the apodization across the pupil realized by SPIRE.

The different locations of the first filter element in SPIRE/PACS also contributes to differences in straylight, e.g. from the thermal shield 2 baffle.

Marginal paths

Many paths found are 'marginal' paths, they involve small solid angles within the path, i.e. a small angular redirection of the rays is sufficient for a blockage of that path. An example is shown in figure 6.4-1 dealing with the mentioned beam limitation on the pupil, i.e. M2. It is clear that the values for the marginal paths have to be considered with caution, since usually only few rays find their way to the detectors due to the small solid angles. Some of these paths are marginal only in terms of solid angle, but not in terms of flux.

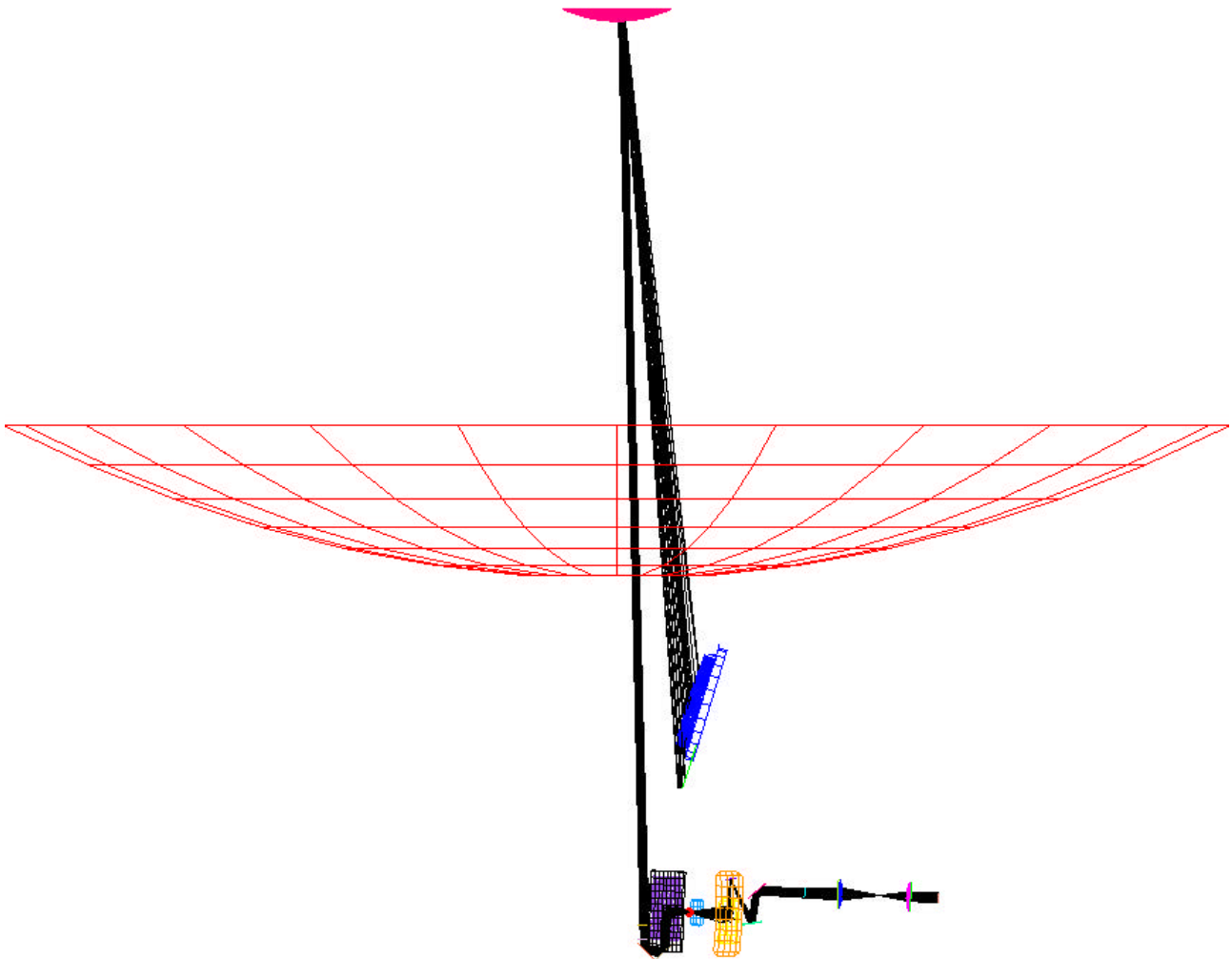


Figure 6.4-1: Marginal path involving the small solid angle of visibility of the M2 surface to the PACS detector.

Sunshade

The contributions from the sunshade have a specular path via the chamfer on the outer rim of M2. If this chamfer is not as regular as it is simulated in the present ASAP model, then this path is reduced to some extent. Presently this path contributes 50% of the value for PACS for the line 'sunshade' (less for SPIRE). Another specular path contributing another 20% for both PACS and SPIRE is via reflection on M1 followed by reflection on the hexapod base in M1 (named M1.FITT_COVER1 in the ASAP file received from ASTRUM France).

Gaps

The emissivity of the gap between sunshade and the outer rim of mirror M1 has been calculated to be only 0.1 (see chapter 5.3) instead of 0.9 as assumed in issue 2. This eliminates the necessity to cover this gap with a low emitting foil.

There are additional black gaps and spaces

- between M1-Baffle cylinder and M1-Baffle cone
- between M1-Baffle cone and CVV top plate
- space on $-Z$ for Cryocover hold down equipment
- space around open Cryocover
- between CVV and Heatshield 2 Baffle
- between Heatshield 2 Baffle and Instrument Shield
- between Instrument Shield and Instruments

which are modelled in the ASAP file

Cryocover black rim

For thermal reasons, the outer rim of the cryocover now is black, in order to avoid the transfer of warm radiation from the gap between CVV and thermal shield 2 baffle onto the instruments during ground test as much as possible.

For sake of completeness, we list the contribution of the deleted version of the earlier black cryocover, i.e. 10% to be added for PACS, 0.4% for SPIRE.

Scattering within instruments

For most cases scattering within the experiments is negligible. The exceptions from that rule are the black thermal shield 2 baffle irradiating SPIRE.

Summary for thermal self emission

The requirement of 10% is violated. The results are 25% for PACS and 13% for SPIRE.

Thermal self emission, optimistic case

Because the requirement is violated by factors of 2.5 for PACS and 1.3 for SPIRE in the pessimistic case, results are given for an optimistic case too. In this optimistic case, the emissivities of reflecting surfaces have been changed from the worst case of 0.05 to an optimistic case of 0.015 and the emissivities of black surfaces have been changed from 0.8 to 0.5. Also the various temperatures of the various objects have been changed to average normal values instead of worst case temperatures plus margin. The results are given in Table 6.4-2.

For the diffraction contribution from the sunshade gap, the lower values for the shorter wavelengths of PACS/SPIRE have been inserted (with the reduced emissivity of 0.08).

For reasons of comparison, one has to leave the contributions from M1 plus M2 on the reference path constant, when comparing the pessimistic and the optimistic case. A reduced emissivity for M1 plus M2 would apparently 'increase' the straylight for the 'optimistic' case, since the large contribution from M1 plus M2 on the reference path is in the denominator of the relative fluxes presented in the tables. Therefore also the sidepaths from M1 plus M2 are unchanged in the table, i.e. not really 'optimistic'. In reality, also these contributions go down for reduced emissivity.

As can be seen, the straylight values for PACS and SPIRE go down to 13.5 % and 8.6 % respectively. For PACS the requirement still is exceeded.

Table 6.4-2: Self emission onto pacs/spire detectors, optimistic case for emissivities (0.015 instead of 0.05 for reflecting surfaces, 0.5 instead of 0.8 for black surfaces, lower temperatures)

Emitting object	temperature/ emissivity	scattering(Sc)/ diffraction(D) on	PACS detector	SPIRE detector
Sunshade	155 K / 0.015	Sc: M1/M2, +spec.	0.451	0.132
gap between. Sunshade and M1	204 K / 0.08	only Sc: M1 / M2	0.154	0.074
gap between. Sunshade and M1	204 K / 0.08	only D: M2(rim)	0.24	0.32
Hexapod	70 K / 0.015		2.334	2.983
M1+M2 (without reference path)	70 K / 0.015		2.488	1.873
scattercone	70 K / 0.015		0.615	0
M1-Baffle flat	64 K / 0.015		0.326	0.274
M1-Baffle cone / cylinder	64 K / 0.015		0.835	0.124
gap (5 mm) between M1-Baffle cone and cylinder	64 K / 0.90		0.506	0.114
Cryocover mirrors	64 K / 0.015		0.160	0.006
other reflecting parts of Cryocover	64 K / 0.015		0.016	0.005
Cryocover black rim	64 K / 0.50		0.860	0.128
reflecting objects near Cryocover	64 K / 0.015		0.109	0.017
black slits around Cryocover / M1-Baffle	64 K / 0.90		2.201	0.344
CVV top	64 K / 0.015		0.292	0.019
gap betw. CVV and Thermal Shield 2 Baffle	64 K / 0.90		0.393	0.099
Thermal Shield 2 Baffle black	40 K / 0.50	only specular	0.804	0.792
Thermal Shield 2 Baffle black	40 K / 0.50	only scattering in instrument	0.039	0.458
Instrument Shield Baffle	12 K / 0.015		0.001	0.001
Gap below Instrument Shield Baffle	12 K / 0.90		0.076	0.033
LOU windows via HiFi	136 K / 0.90		0.042	0.036
LOU windows via heat shield gaps	136 K / 0.90		0.195	0.017
Holes in OB for cooling straps (worst case consideration only)	34 K / 0.90		0.2	0.02
sum			13.3	7.9

Data for PACS and SPIRE are in % with 100% = telescope irradiation (70 K, total $\epsilon=0.03$)

7 Sources outside the FOV (Sun, Earth, Moon)

7.1 Specular paths from Moon and Earth

There are some specific directions from which the Moon or the Earth can be reflected specularly via various hexapod structures into the instrument detectors. These specular paths from moon/earth found during the calculations for issue 1 led to the recommendation of rounding the legs of the hexapod assembly. As already mentioned, the elliptical legs of the telescope are approximated with a polygonal cross section with 24 sides. Therefore slim plane surfaces exist in the model whereas the reality will be a curved surface. The polygonal modelling has the advantage to highlight paths which might be overlooked with curved surfaces (due to insufficient ray statistics), thus is very helpful. However these paths could be overestimated.

The specular paths found for the elliptical version are more spreaded over the sky, however they represent less sensitive paths. A comment from the scientists states that the minor degree of spreading is favoured, so the calculations of the earlier issue 1 (performed with the version with rectangular legs) are reported here again.

The changes mentioned in chapter 4.3 (new inclination of the hexapod bar, new center ring of the M1-baffle) do not change the overall picture, however the specular paths exist for somewhat different directions.

Most of the specular directions are close to the limit for the possible moon directions, at around 20 degrees from the X-axis; therefore they are affected by the Moon (and bright stars) only and not by the Earth.

Figure 7.1-1 shows these directions for the case of the SPIRE detector, figure 7.1-2 displays the case of the PACS detector. Both are gained by a backward trace.

Two of the most important paths for SPIRE are shown in figure 7.1-3 and figure 7.1-4

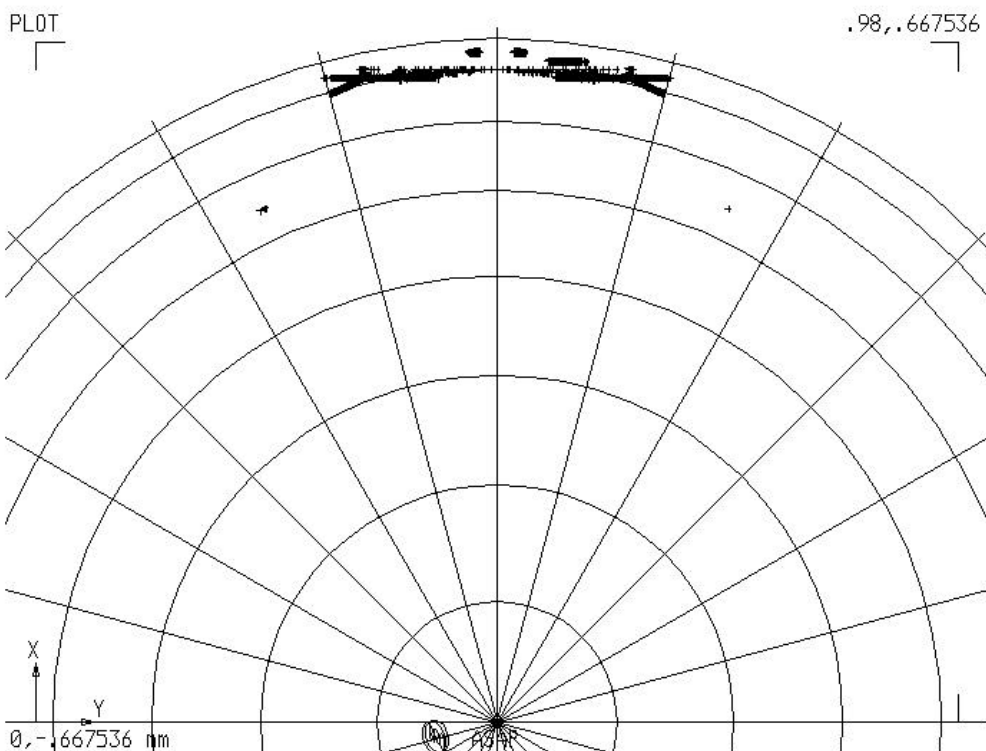


Figure 7.1-1: Directions from which specularly reflected rays can hit the SPIRE detector.

Plot of directions towards the sky. The center of this polar diagram is the +Z axis. The circles around the +Z axis have distances of 10 degrees.

The outermost line roughly represents the limiting direction for the moon.

The limit for the earth is between the 2nd and the 3rd circle from outside.

Each + sign represents a direction with specular paths towards the SPIRE detector

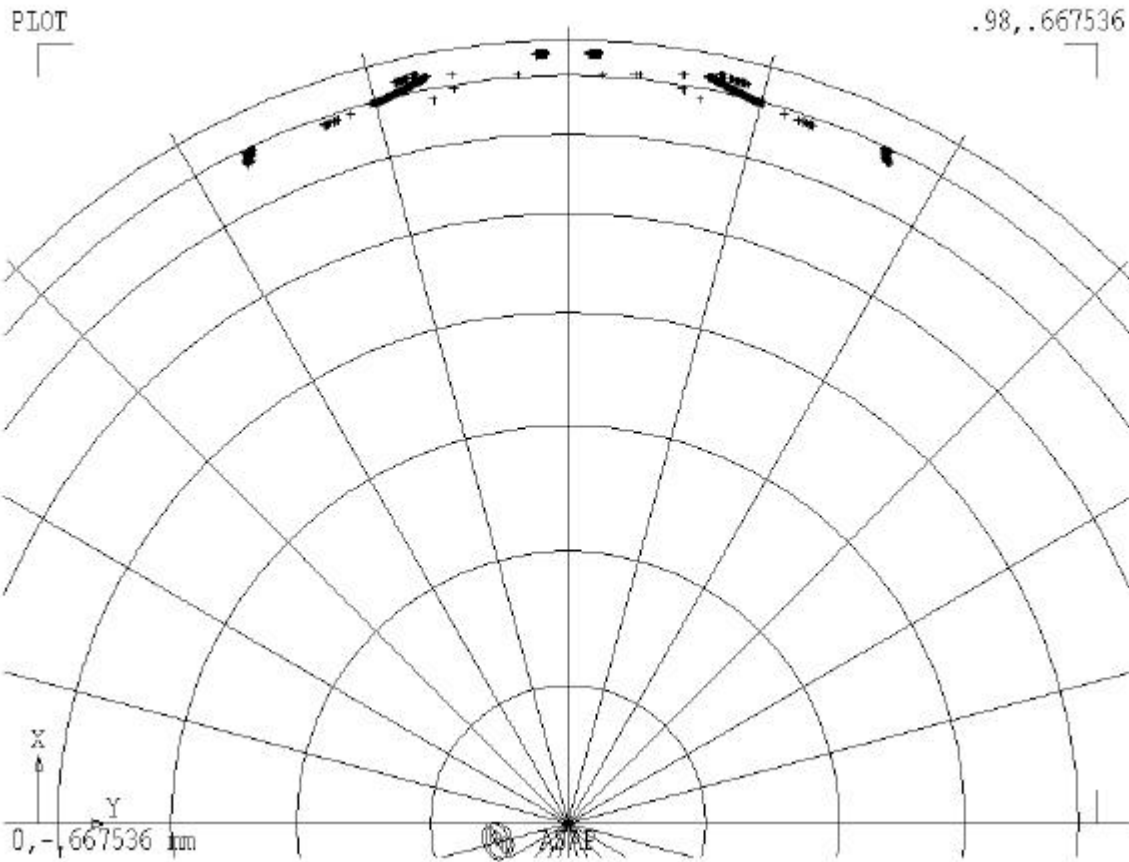


Figure 7.1-2: Directions from which specularly reflected rays can hit the PACS detector.

Plot of directions towards the sky. The center of this polar diagram is the +Z axis. The circles around the +Z axis have distances of 10 degrees.

The outermost line roughly represents the limiting direction for the moon.

The limit for the earth is between the 2nd and the 3rd circle from outside.

Each + sign represents a direction with specular paths towards the PACS detector

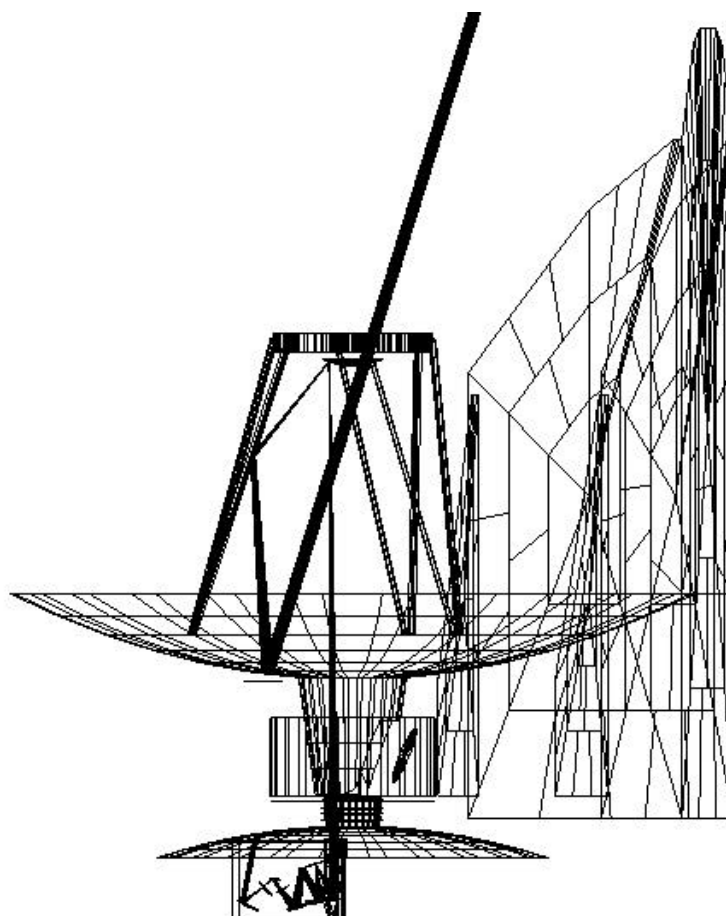


Figure 7.1-3: Specular Straylight path no. 1 for the moon

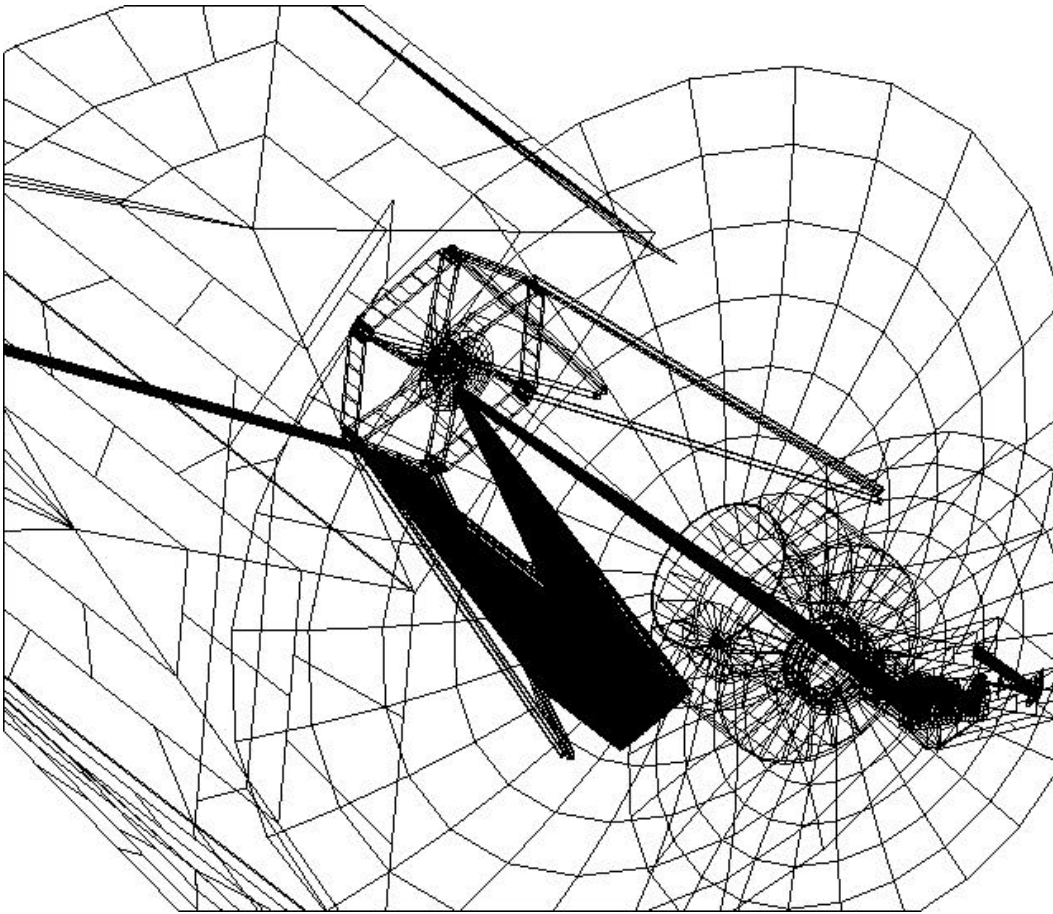


Figure 7.1-4: Specular straightlight path no. 3 for the moon

Table 7.1-1 shows averaged coordinates and directions of some of the detected direct paths for the SPIRE detector. The directions are those plotted in figure 7.1-1. The coordinates are the averaged positions on Herschel, where rays on the specific path hit the first Herschel object (e.g. a hexapod strut, mirror M1, etc.).

path		coordinates of grid.			directions of source		
		X	Y	Z	A	B	C
1	M1-Z	1297.47	284.46	-429.13	-.9189013081	-.2136134569	-.3310044862
2	M1-Z	1297.53	-285.06	-427.56	-.9189812584	.21347118273	-.3308537199
3	HEX-Y	2928.56	-301.65	237.96	-.9406922184	.13956008227	-.3089975805
4	HEX+Y	2928.08	302.04	237.28	-.9406708956	-.1409893138	-.308641475

Table 7.1-1: Average coordinates and directions for the most important direct paths onto SPIRE detector

The radiation onto the SPIRE detector was calculated for paths no. 1, 2 and 3. Path 4 is symmetric to path 3, and therefore is expected to give similar results. All other paths show less radiation in the backward trace, and therefore are expected to give lower results.

Moon and Earth are treated as extended sources with angular radius of 0.002 and 0.005 rad, they are placed in a distance of 1,000,000 mm from the telescope, which is sufficient for the ASAP calculations. They are lambertian sources with emissivity 1, scattering towards the telescope targets. The Moon has such an angular extension that it covers most of the pixels of PACS and SPIRE detectors. Therefore the relative comparison to the telescope radiation is done by comparing radiances of moon and telescope and by division of the ASAP fluxes onto the detectors as in the case of self emission.

Results:

The paths result in real images on the detector. Paths 1 and 2 are somewhat diffuse, path 3 represents a sharp picture. All paths shown in the following table are potential paths for the Moon.

relative flux on SPIRE detector	path 1 and 2	1.5E-3 each
relative flux on SPIRE detector	path 3	1.9E-3.
contribution from M1 + M2 onto SPIRE detector	reference path	16.4

The contributions from these paths have to be corrected for temperature and for emissivity in order to do a correct comparison with the telescope. The assumed emissivity and temperature of telescope mirrors are 0.015 and 70 K each. The assumed emissivities and temperatures of the moon are 1 (black body), 100 K for the dark region, 400 K for the illuminated region (consistent with RD 2).

The contributions for all moon paths therefore have to be corrected by the following factors:

	Moon bright zone (400 K)		Moon dark zone (100 K)	
	80 μ	670 μ	80 μ	670 μ
temperature factor (=1 for 70 K)	21.25	6.55	2.39	1.50
emissivity factor	66.67	66.67	66.67	66.67
Total multiplication factor	1417	437	159	100

Table 7.1-2: Correction factors for ASAP results concerning the Moon.

The comparison to the telescope background therefore gives (in % of M1 + M2 straylight):

	Moon bright zone (400 K)		Moon dark zone (100 K)	
	80 μ	670 μ	80 μ	670 μ
Path 1	13.0%	4.0%	1.45%	0.92%
Path 2	13.0%	4.0%	1.45%	0.92%
Path 3	16.4%	5.1%	1.84%	1.16%

Table 7.1-3: Contributions from Moon on SPIRE detector for paths 1 - 3

Thus the specification of 1% is violated. The situation for PACS is similar as verified independently by ALCATEL (RD3).

The possible means for an improvement of the situation have not been introduced, see explanation given above.

Remark: The specular paths probably exist also towards other directions onto the sky due to the symmetry of the hexapod structure. There moon and earth will never appear, nevertheless planets and bright stars may reach these patches of the sky. Beam chopping and nodding will be affected. The rounding of the hexapod structures (mentioned above for the case of the moon patches) will also improve the situation for chopping and nodding. Maps displaying these directions can be found in RD 1.

7.2 Scatter Paths from Moon and Earth

All results are presented as relative numbers w.r.t. the thermal radiation of the telescope mirrors M1 and M2.

Their contribution has been set to 100 so the violation of the requirement of 1% for moon/earth occurs if the numbers exceed 1.

The table shows that the scatter paths (scatter at primary and secondary mirror) are negligible. Thus only the patches mentioned in section 7.1 violate the specification.

Table 7.2-1: Scatter paths from moon/earth onto pacs and spire detector

emitting object	PACS DETECTOR	area= 1320 mm ²	SPIRE DETECTOR	area= 902 mm ²
	flux	irradiance	flux	irradiance
moon at 13 degrees, cone baffle	8.69E-04	8.69E-04	5.00E-04	5.00E-04
moon at 13 degrees, cylinder baffle	8.09E-04	8.09E-04	4.37E-04	4.37E-04
earth at 23 degrees, cone baffle	4.09E-03	4.09E-03	1.81E-03	1.81E-03
earth at 23 degrees, cylinder baffle	4.22E-03	4.22E-03	1.72E-03	1.72E-03

The results reported here are those of issue 1, they have not been recalculated for the changes introduced since then:

- combined cylinder/cone baffle
- new mirror scattering function
- SPIRE apodization.

Since the numbers are so low, there is no danger for approaching the specified value of 1%, if a recalculation is done.

7.3 Solar irradiation

The diffraction of the solar radiation at the sunshade yields irradiances small compared to the specification as elaborated in RD1.

8 Sources inside the FOV

No calculations were made by ASED. The subject has been already treated by ASEF in RD1. The results from ASEF show compliance with the specification with good margin.

The question of cross-talk between SPIRE and PACS has been treated in RD3. For an assumed residual reflection of 10% on the SPIRE detector the in-field requirement is still met with margin.

9 Summary of Changes not fully reflected by present Calculations

The flat ring above the cylindrical part of the M1-baffle is part of all calculations in this issue 3. A very recent change is the wish of HIFI for a conical shape of the innermost flat part of the M1-baffle. Meanwhile the flat shape has been abandoned and it was decided to give an upwards angle of 3.5 degrees +/- 2 degrees for the upper flat part of the M1 central baffle. The consequences are estimated to be small for general straylight, since it has been verified that no additional purely specular paths are introduced by this change.

The new inclinations of the hexapod bar (and the change mentioned above) will alter the directions found for the specular paths from moon and earth (also for those in RD1). They do not change the overall picture, however the specular paths exist for somewhat different directions. The differences in direction are important for mission planning.

10 Summary on Straylight

Summary for thermal self emission:

The requirement of 10% is violated. Possible improvements (large scattercone) have not been introduced because of disadvantageous obscuration.

Summary for out-of-field Sources (Sun, Earth, and Moon):

This radiation is within specification, except for small locations on the sky, where radiation reflected at rectangular hexapod structures can enter the instruments directly. These small locations exist mainly for the Moon. Only two minor paths were found which could be applicable also for the Earth. For the worst case locations of the Moon the specification is exceeded by about a factor of up to 17.

Note: Because these straylight paths partially lead to sharp ghost images on the detector, even bright stars/planets on these locations could influence chopping and nodding. There are much more dangerous locations for bright stars than for moon and earth.

Summary for in-field Sources:

The requirement is met.

11 Appendix: Scattering Models used for the Calculations

The following pictures show the scattering models used for the calculations.

Models for Telescope and Cyostat parts (Figures 11.1-1 through 11.1-3)

PACS scatter model (Figure 11.2-1)

SPIRE scatter models (Figures 11.3-1 through 11.3-5)

In addition, a Lambertian model ($BSDF=0.1/\pi$ per sr) was used for

- the filter in the PACS pupil (in transmission)
- PACS mechanics around the PACS opening.

(model not shown as picture).

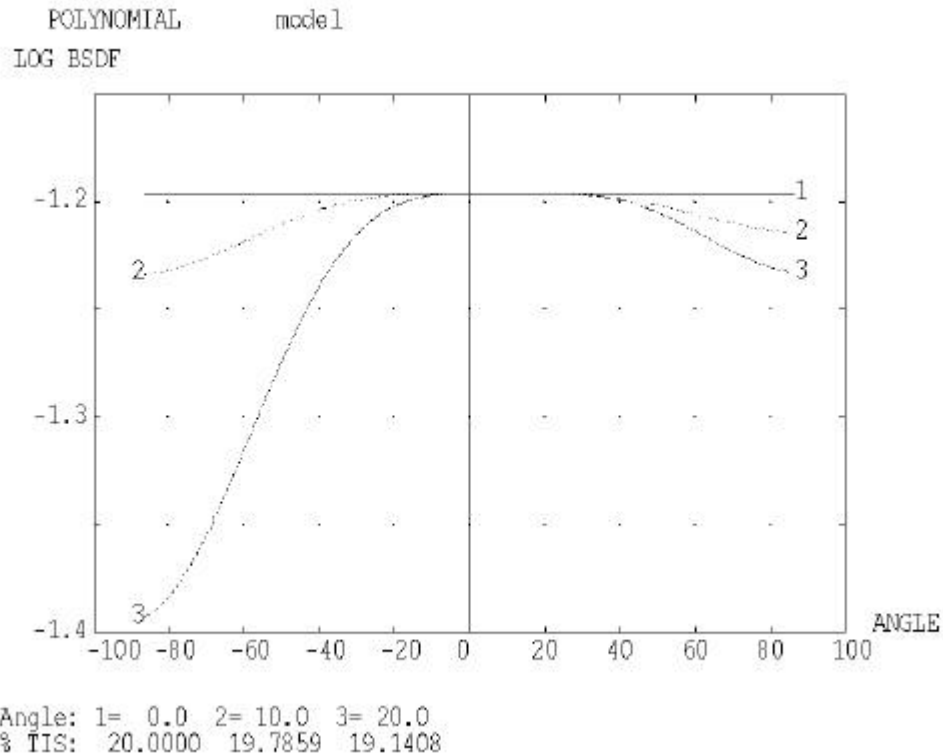
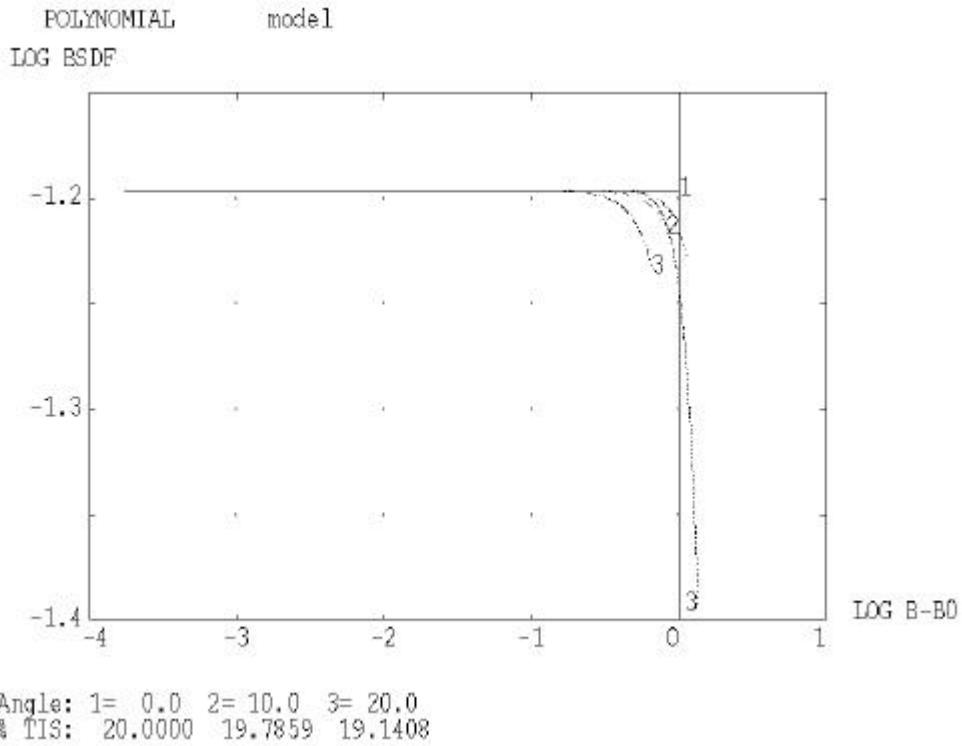


Fig. 11.1-1: Model for thermal shield 2 baffle and instrument shield baffle tube (also for deleted black flat cryocover variant)
 (POLYNOMIAL 2 2 LOG[.2/3.1416] 5@0, 0 0 1.8 0 0 1.8, 0 -1.8)
 The upper plot mainly shows the values for small scattering angles
 The lower plot mainly shows the values for large scattering angles

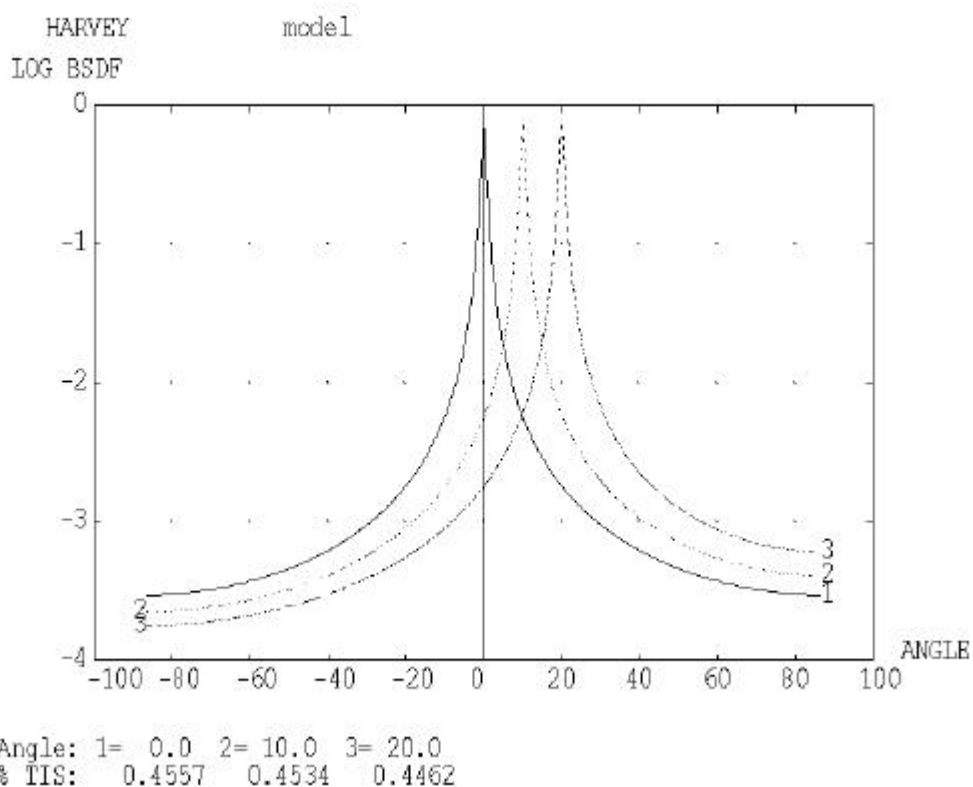
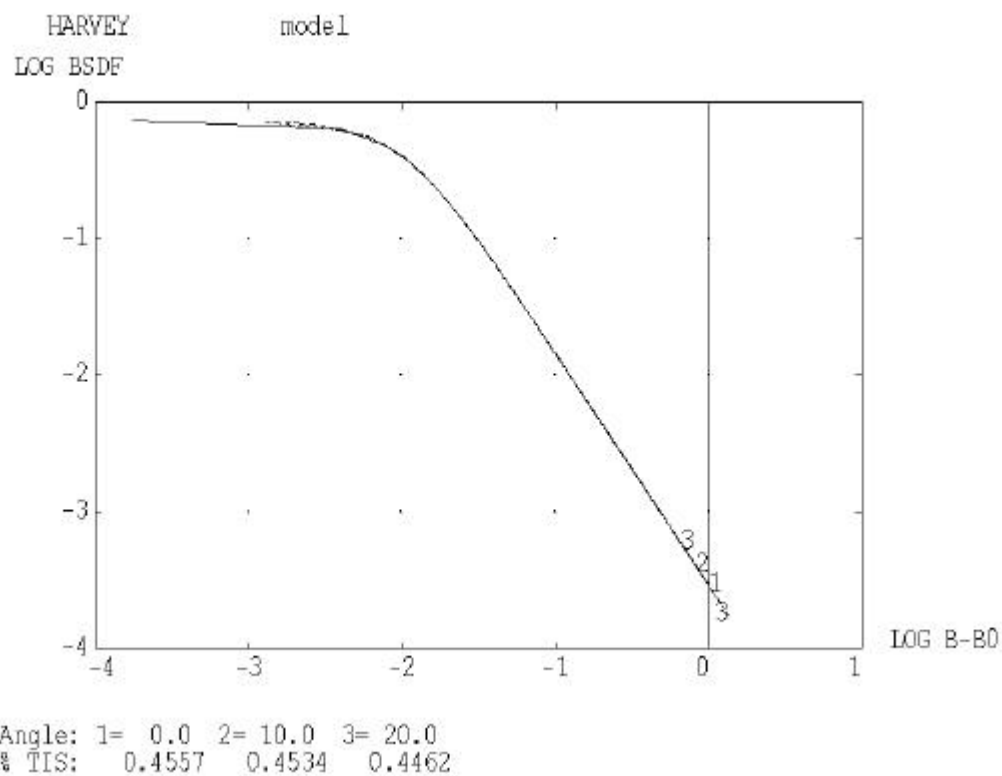


Fig. 11.1-2: Model for telescope mirrors, Harvey 0.73 -1.7 0.01
 The upper plot mainly shows the values for small scattering angles
 The lower plot mainly shows the values for large scattering angles

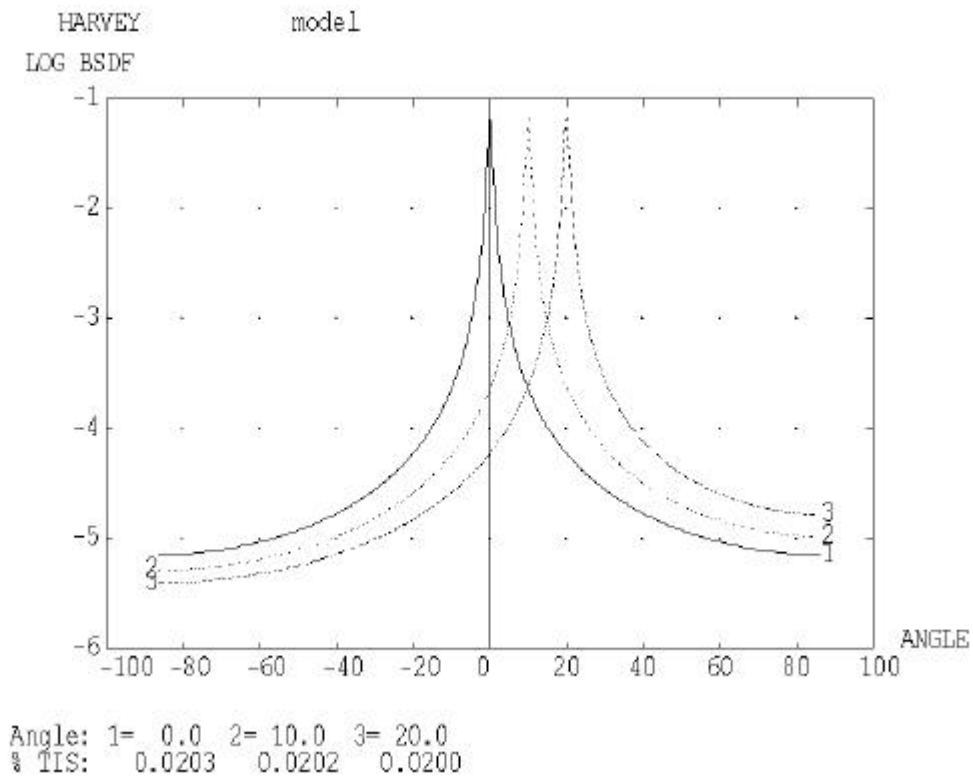
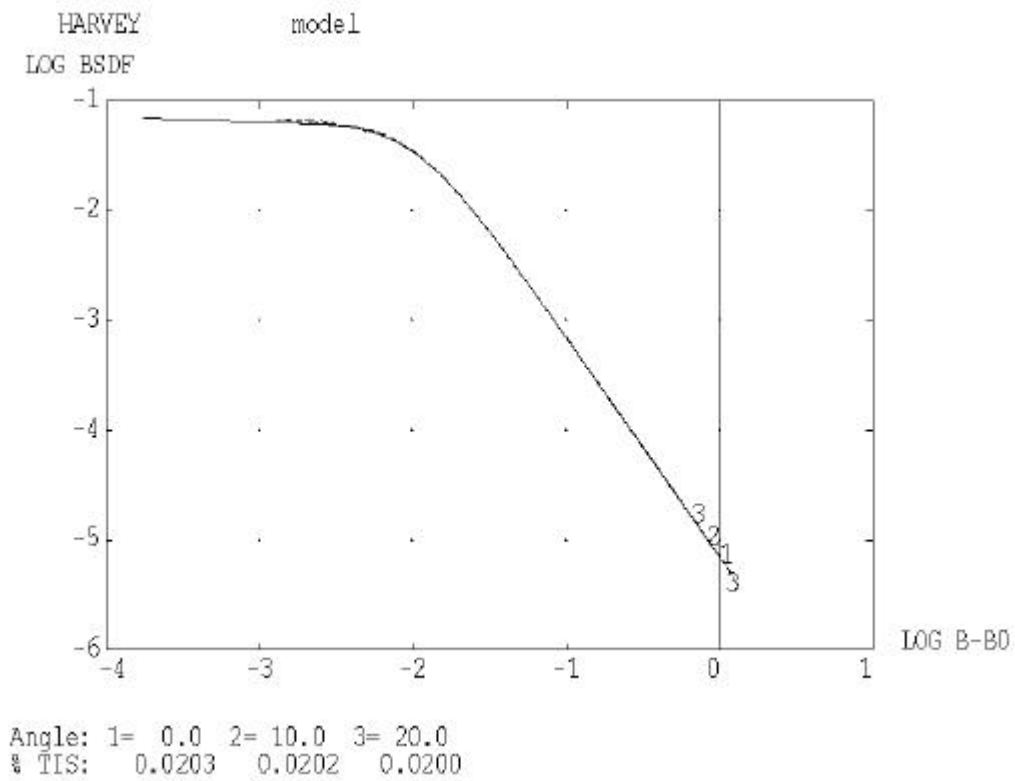


Fig. 11.1-3: Model for instrument shield flat and flat cryocover parts, Harvey 0.07 -2 0.01
The upper plot mainly shows the values for small scattering angles
The lower plot mainly shows the values for large scattering angles

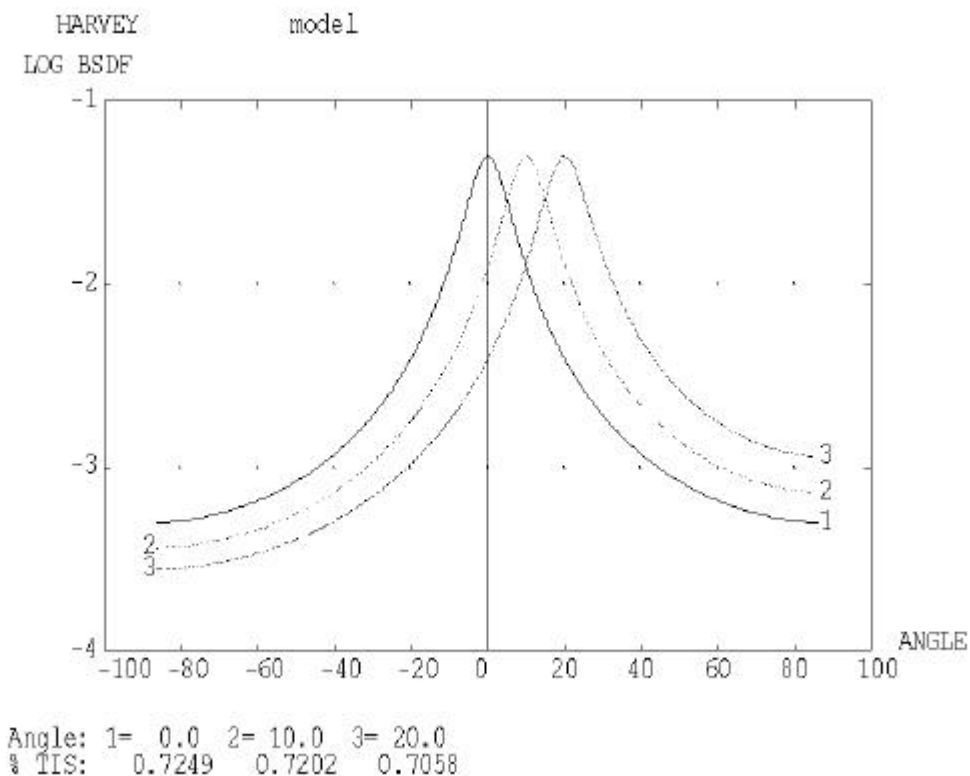
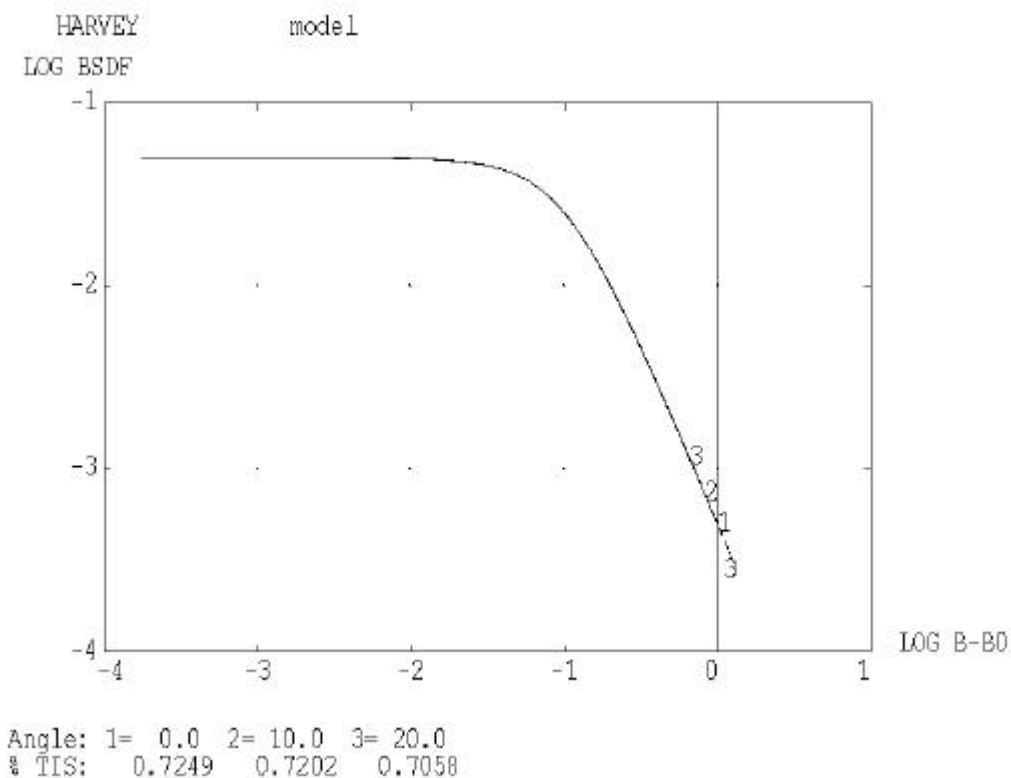


Fig. 11.2-1: Model for PACS Trog1, Trog2, Trog3, Fold1, Harvey 0.05 -2 0.1
 The upper plot mainly shows the values for small scattering angles
 The lower plot mainly shows the values for large scattering angles

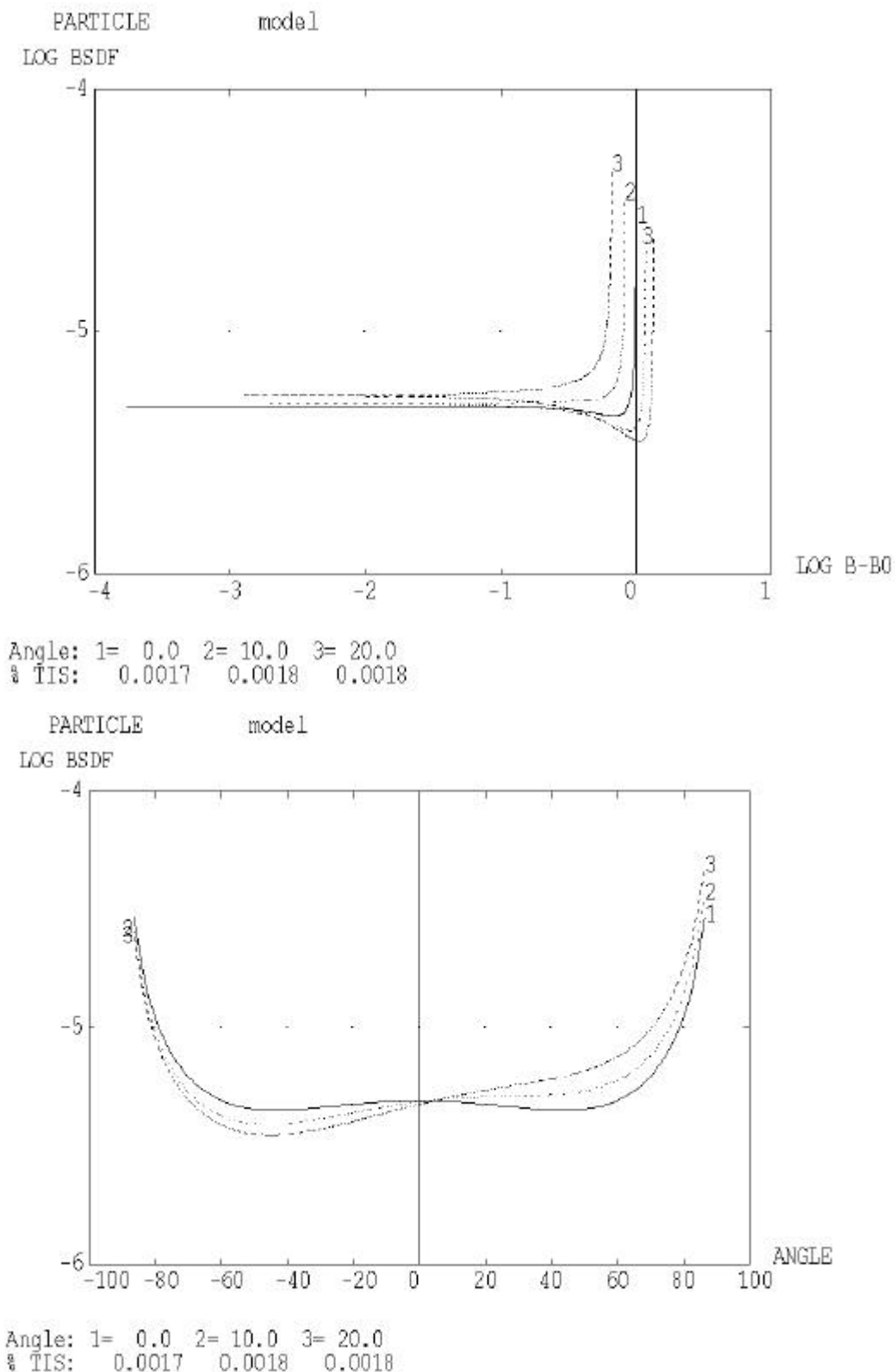


Fig. 11.3-1: Model for SPIRE mirrors, especially M3 (particle model),
 The upper plot mainly shows the values for small scattering angles
 The lower plot mainly shows the values for large scattering angles

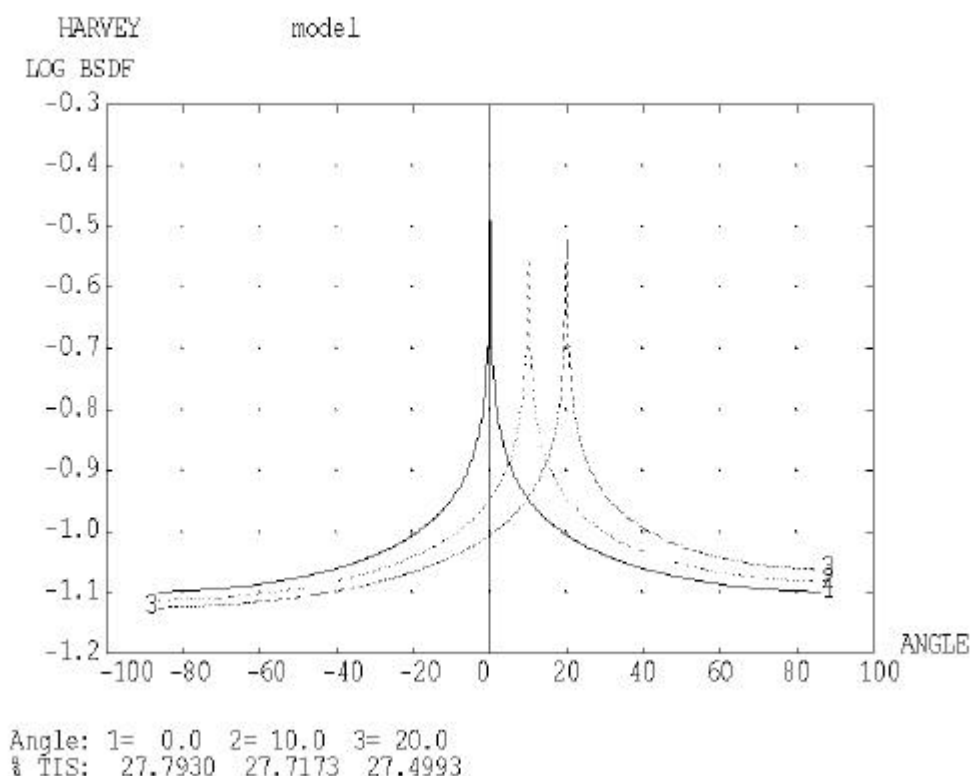
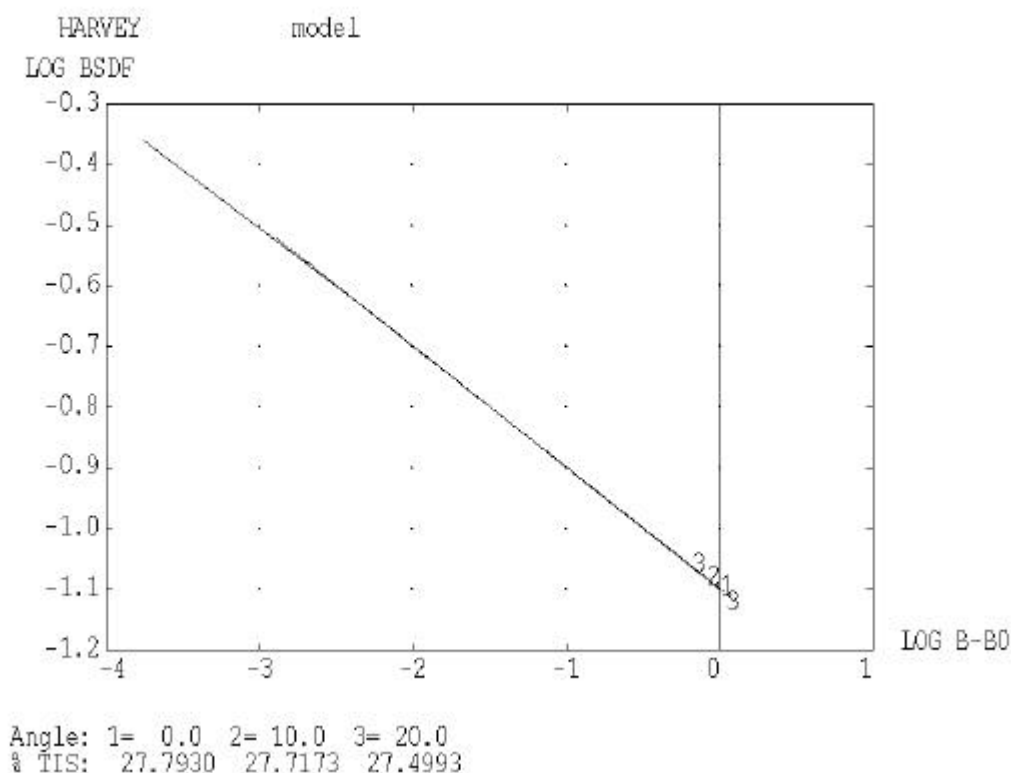


Fig. 11.3-2: Model for SPIRE M4 aperture (i.e. mechanics around M4), Harvey 0.2 -0.2
 The upper plot mainly shows the values for small scattering angles
 The lower plot mainly shows the values for large scattering angles

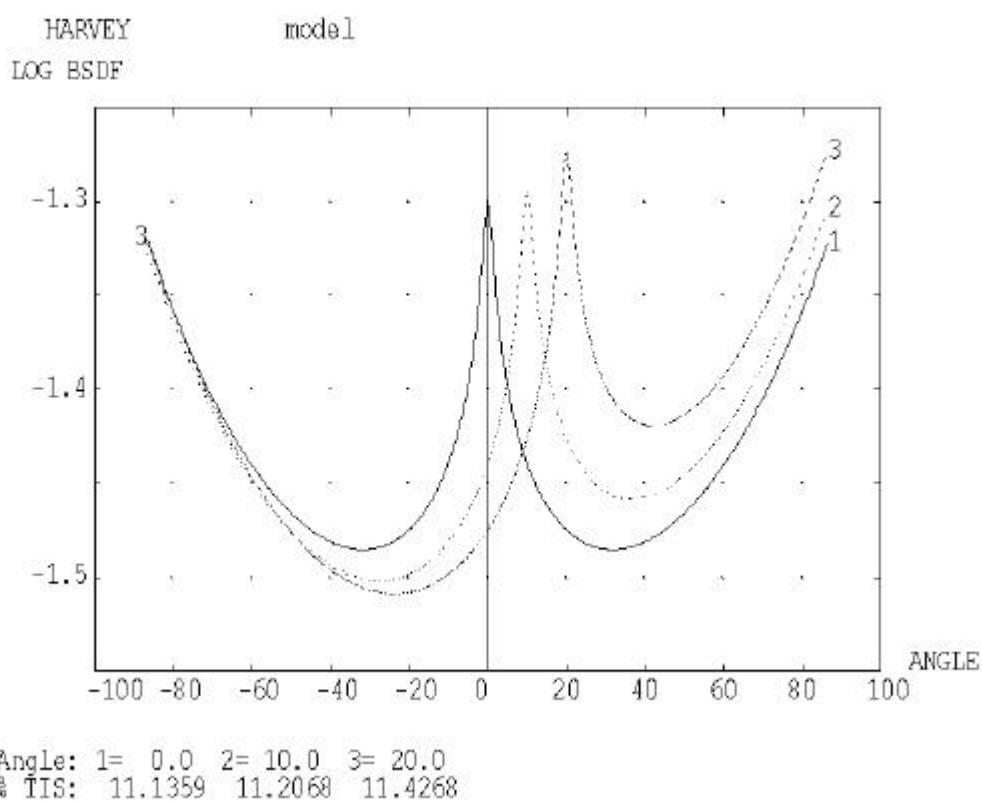
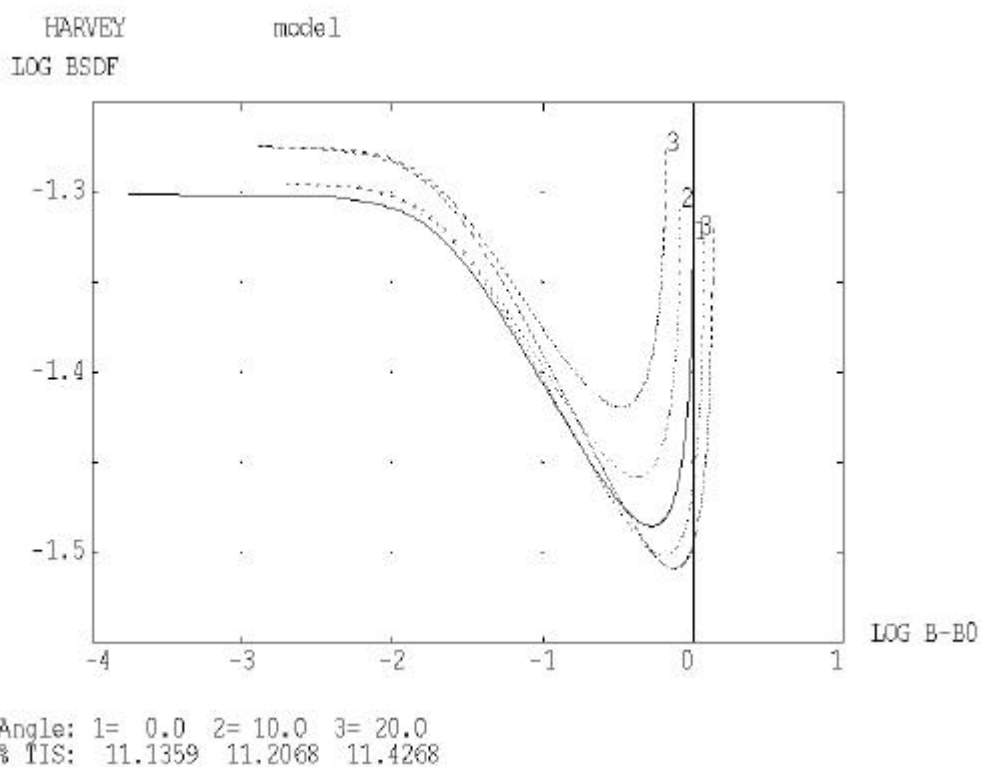
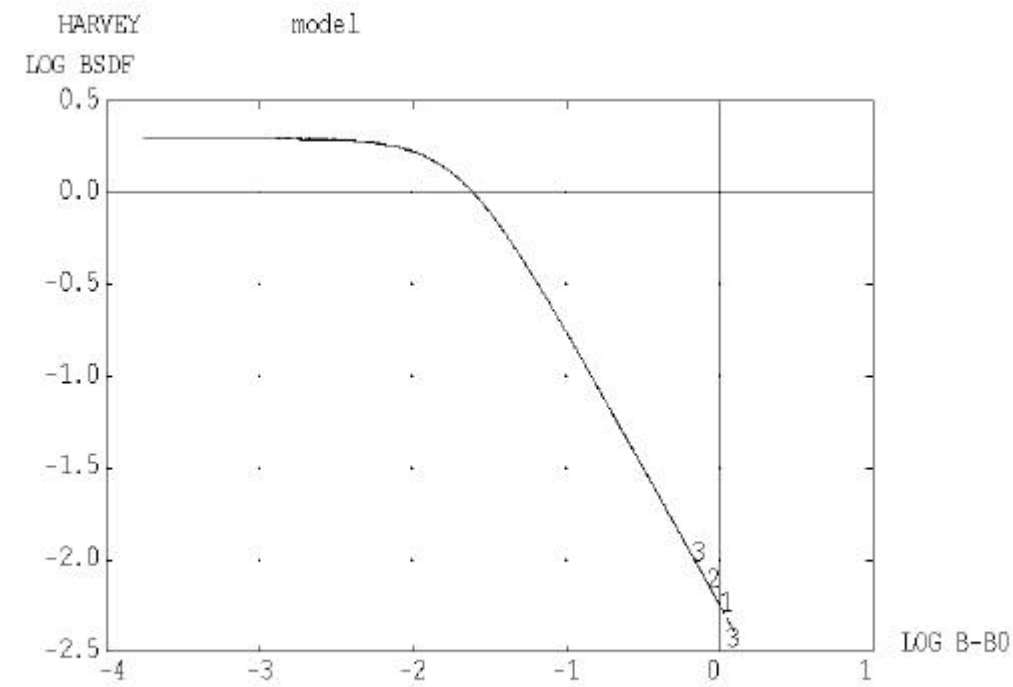
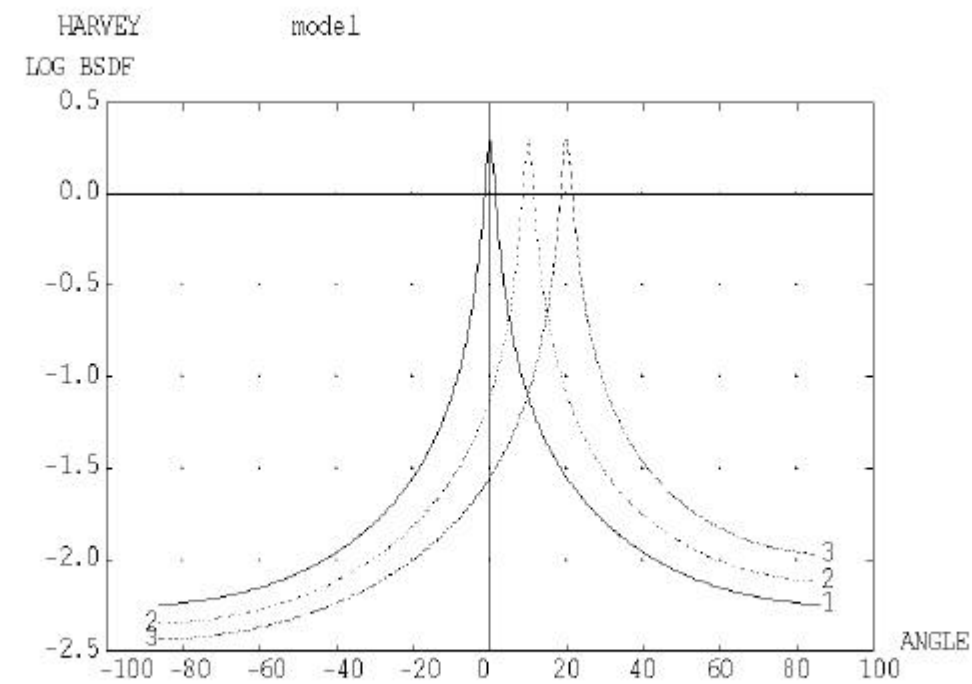


Fig. 11.3-3: Model for SPIRE FP_UNIT, upper part, HARVEY 0.05 -0.15 0.02 1 1
The upper plot mainly shows the values for small scattering angles
The lower plot mainly shows the values for large scattering angles

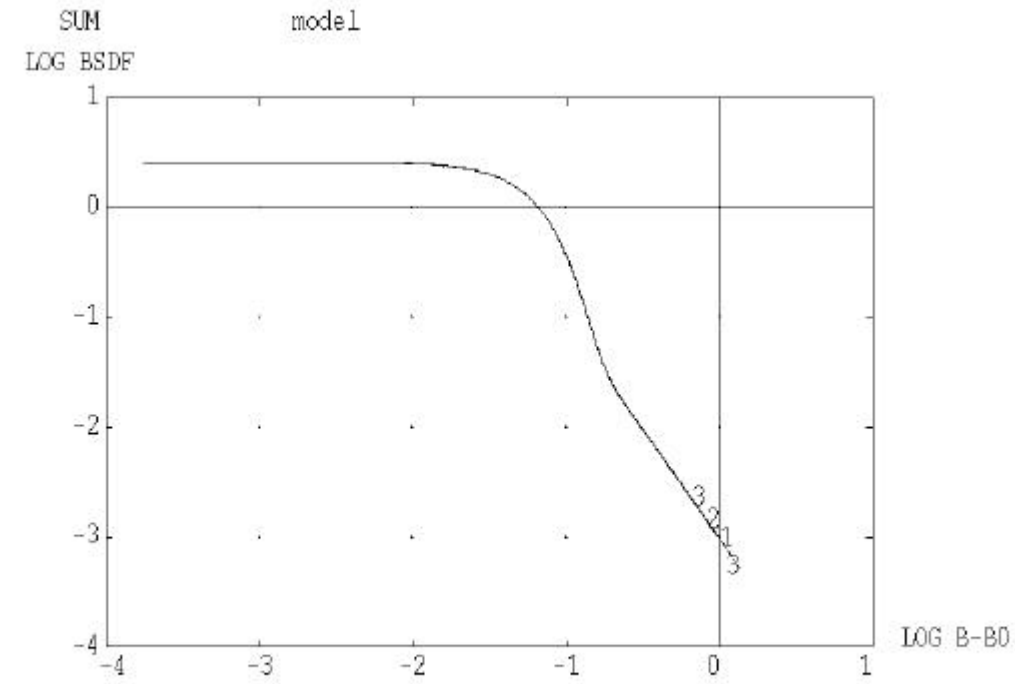


Angle: 1= 0.0 2= 10.0 3= 20.0
 % TIS: 6.1035 6.0630 5.9414

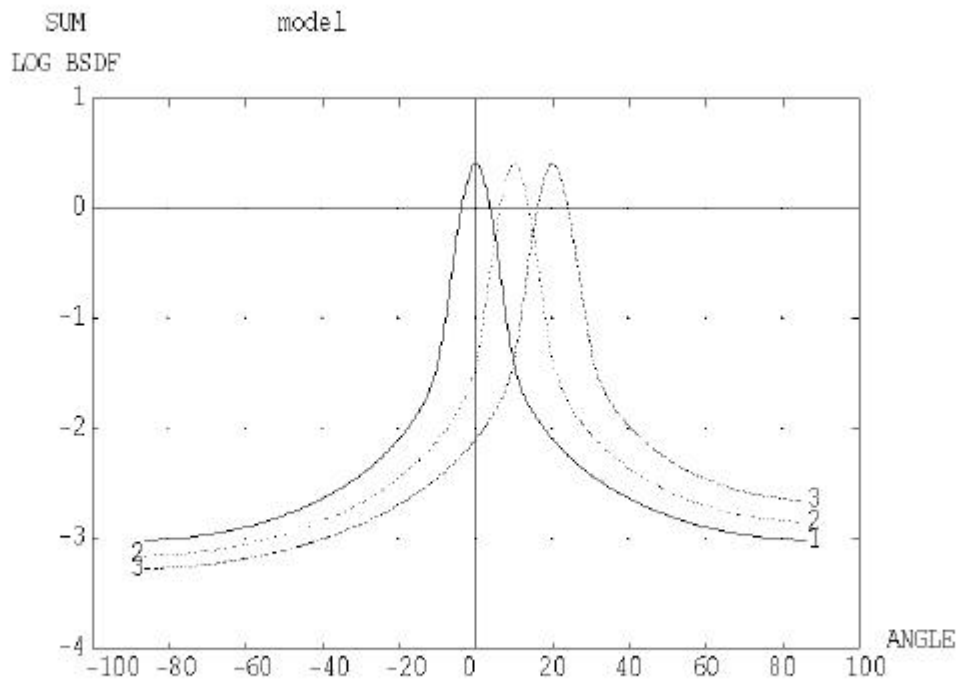


Angle: 1= 0.0 2= 10.0 3= 20.0
 % TIS: 6.1035 6.0630 5.9414

Fig. 11.3-4: Model for SPIRE FP_UNIT, lower part, HARVEY 2 -1.5 0.02
 The upper plot mainly shows the values for small scattering angles
 The lower plot mainly shows the values for large scattering angles



Angle: 1= 0.0 2= 10.0 3= 20.0
% TIS: 5.1486 5.1394 5.1112



Angle: 1= 0.0 2= 10.0 3= 20.0
% TIS: 5.1486 5.1394 5.1112

Fig. 11.3-5: Model for SPIRE filter 1, sum of Harvey 2.0 -50 0.35 and Harvey 0.60 -2.0 0.04
The upper plot mainly shows the values for small scattering angles
The lower plot mainly shows the values for large scattering angles

END OF DOCUMENT

Name	Dep./Comp.	Name	Dep./Comp.
Alberti von Mathias Dr.	SM 34	Schweickert Gunn	SM 34
Alo Hakan	OTN/LP 45	Stauss Oliver	SM 33
Barlage Bernhard	ED 11	Steininger Eric	ED 422
Bayer Thomas	ED 541	Stritter Rene	ED 11
Faas Horst	EA 65	Suttner Klaus	SM 32
Fehringer Alexander	SM 33	Tenhaeff Dieter	SM 34
Frey Albrecht	ED 422	Thörmer Klaus -Horst Dr.	OTN/ED 65
Gerner Willi	ED 11	Wagner Adalbert	OTN/LP 45
Grasl Andreas	OTN/EN 64	Wagner Klaus	SM 31
Grasshoff Brigitte	ED 521	Wietbrock, Walter	ED 521
Hartmann Hans Dr.	ED 422	Wöhler Hans	SM 34
Hauser Armin	SM 31	Zipf Ludwig	ACE 32
Hinger Jürgen	SM 31		
Hohn Rüdiger	ED 541		
Hölzle Edgar	ED 421	Alcatel	ASP
Huber Johann	ED 543	ESA/ESTEC	ESA
Hund Walter	SE 76		
Idler Siegmund	ED 432	Instruments:	
Ivány von András	ACE 32	MPE (PACS)	MPE
Jahn Gerd Dr.	SM 31	RAL (SPIRE)	RAL
Kalde Clemens	ED 532	SRON (HIFI)	SRON
Kameter Rudolf	OTN/EN 64	Subcontractors:	
Kersting Stefan	OTN/EN 63	Air Liquide, Space Department	AIR
Kettner Bernhard	SM 34	Air Liquide, Space Department	AIRS
Knoblauch August	ED 531	Air Liquide, Orbital System	AIRT
Koelle Markus	ED 523	Alcatel Bell Space	ABSP
Kroeker Jürgen	ED 542	Astrium Sub-Subsyst. & Equipment	ASSE
Kunz Oliver	SM 31	Austrian Aerospace	AAE
Lamprecht Ernst	OTN/SM 222	Austrian Aerospace	AAEM
Lang Jürgen	SE 76	APCO Technologies S. A.	APCO
Langfermann Michael	ED 541	Bieri Engineering B. V.	BIER
Mack Paul	OTN/EN 64	BOC Edwards	BOCE
Muhl Eckhard	OTN/EN 64	Dutch Space Solar Arrays	DSSA
Pastorino Michel	ASPI Resid.	EADS CASA Espacio	CASA
Peitzker Helmut	ED 65	EADS CASA Espacio	ECAS
Peltz Heinz-Willi	SM 33	EADS Space Transportation	ASIP
Peters, Gerhard	ED 531	Eurocopter	ECD
Pietroboni Karin	ED 65	HTS AG Zürich	HTSZ
Puttlitz Joachim	OTN/EN 64	Linde	LIND
Rebholz Reinhold	ED 541	Patria New Technologies Oy	PANT
Reuß Friedhelm	ED 62	Phoenix, Volkmarsen	PHOE
Rühe Wolfgang	ED 6	Prototech AS	PROT
Runge Axel	OTN/EN 64	QMC Instruments Ltd.	QMC
Sachsse Bernt	ED 21	Rembe, Brilon	REMB
Schäffler Johannes	OTN/EN 64	SENER Ingenieria SA	SEN
Schink Dietmar	ED 422	Stöhr, Königsbrunn	STOE
Schlosser Christian	OTN/EN 64	Rosemount Aerospace GmbH	ROSE
Schmidt Rudolf	ACE 32	RYMSA, Radiación y Microondas S.A.	RYM